

# UC Davis

## UC Davis Previously Published Works

### Title

Enhanced Depolarization Drive in Failing Rabbit Ventricular Myocytes

### Permalink

<https://escholarship.org/uc/item/7dw252cn>

### Journal

Circulation Arrhythmia and Electrophysiology, 12(3)

### ISSN

1941-3149

### Authors

Hegy, Bence

Morotti, Stefano

Liu, Caroline

et al.

### Publication Date

2019-03-01

### DOI

10.1161/circep.118.007061

Peer reviewed



Published in final edited form as:

*Circ Arrhythm Electrophysiol.* 2019 March ; 12(3): e007061. doi:10.1161/CIRCEP.118.007061.

## Enhanced Depolarization Drive in Failing Rabbit Ventricular Myocytes: Calcium-dependent and $\beta$ -Adrenergic Effects on Late Sodium, L-type Calcium and Sodium-Calcium Exchange Currents

Bence Hegyi, MD, PhD<sup>1</sup>, Stefano Morotti, PhD<sup>1</sup>, Caroline Liu<sup>1</sup>, Kenneth S. Ginsburg, PhD<sup>1</sup>, Julie Bossuyt, DVM, PhD<sup>1</sup>, Luiz Belardinelli, MD<sup>2</sup>, Leighton T. Izu, PhD<sup>1</sup>, Ye Chen-Izu, PhD<sup>1,3,4</sup>, Tamás Bányász, MD PhD<sup>1,5</sup>, Eleonora Grandi, PhD<sup>1</sup>, Donald M. Bers, PhD<sup>1</sup>

<sup>1</sup>Department of Pharmacology, University of California Davis, Davis

<sup>2</sup>Former employee of Gilead Sciences, Inc., Foster City, CA

<sup>3</sup>Department of Biomedical Engineering, University of California Davis, Davis

<sup>4</sup>Department of Internal Medicine/Cardiology, University of California Davis, Davis

<sup>5</sup>Department of Physiology, Faculty of Medicine, University of Debrecen, Debrecen, Hungary

### Abstract

**Background:** Heart failure (HF) is characterized by electrophysiological remodeling resulting in increased risk of cardiac arrhythmias. Previous reports suggest that elevated inward ionic currents in HF promote action potential (AP) prolongation, increased short-term variability of AP repolarization (STV) and delayed afterdepolarizations. However, the underlying changes in late Na<sup>+</sup>, L-type Ca<sup>2+</sup>, and Na<sup>+</sup>/Ca<sup>2+</sup> exchanger currents ( $I_{NaL}$ ,  $I_{CaL}$  and  $I_{NCX}$ , respectively) are often measured in nonphysiological conditions (square pulse voltage-clamp, slow pacing rates, exogenous Ca<sup>2+</sup> buffers).

**Methods:** We measured the major inward currents and their Ca<sup>2+</sup>- and  $\beta$ -adrenergic dependence under physiological AP-clamp in rabbit ventricular myocytes in chronic pressure/volume overload-induced HF (versus age-matched control).

**Results:** AP duration and STV were increased in HF, and importantly, inhibition of  $I_{NaL}$  decreased both parameters to the control level.  $I_{NaL}$  was slightly increased in HF versus control even when intracellular Ca<sup>2+</sup> was strongly buffered. But under physiological AP-clamp with normal Ca<sup>2+</sup> cycling,  $I_{NaL}$  was markedly upregulated in HF versus control (dependent largely on Ca<sup>2+</sup>/calmodulin-dependent protein kinase II (CaMKII) activity).  $\beta$ -adrenergic stimulation (often elevated in HF), further enhanced  $I_{NaL}$ .  $I_{CaL}$  was decreased in HF when Ca<sup>2+</sup> was buffered, but CaMKII-mediated Ca<sup>2+</sup>-dependent facilitation upregulated physiological  $I_{CaL}$  to the control level.

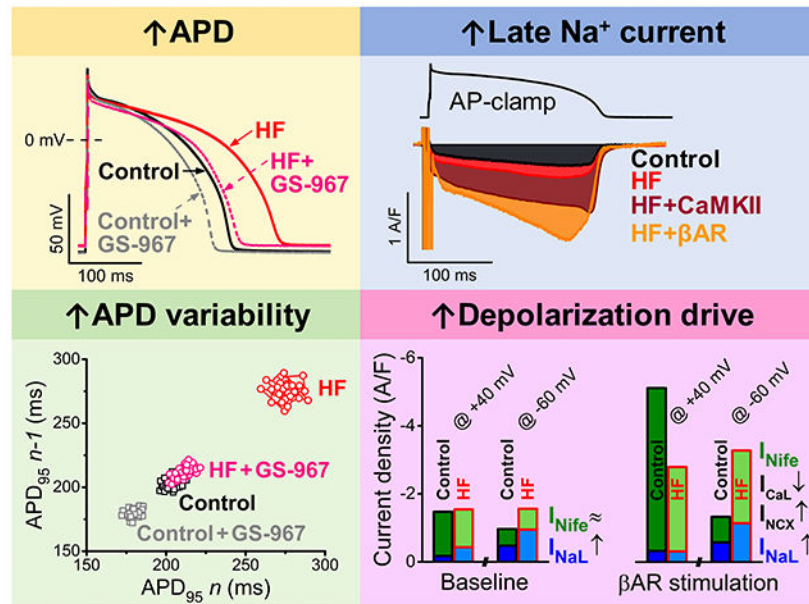
**Correspondence:** Donald M. Bers, PhD, Department of Pharmacology, University of California, Davis, 451 Health Sciences Dr, Davis, CA 95616, Tel: (530) 752-6517, Fax: (530) 752-7710, dmbers@ucdavis.edu.

**Disclosures:** Dr Luiz Belardinelli is a former employee of Gilead Sciences, Inc, which is the patent holder of GS-967. Current affiliation of Dr Belardinelli is InCarda Therapeutics, Inc. (Brisbane, CA, USA). The authors declare that they have no conflict of interest.

Furthermore,  $I_{CaL}$  response to  $\beta$ -adrenergic stimulation was significantly attenuated in HF. Inward  $I_{NCX}$  was upregulated at phase 3 of AP in HF when assessed by combining experimental data and computational modeling.

**Conclusions:** Our results suggest that CaMKII-dependent upregulation of  $I_{NaL}$  in HF significantly contributes to AP prolongation and increased STV, which may lead to increased arrhythmia propensity, and is further exacerbated by adrenergic stress.

## Graphical Abstract



## Keywords

electrophysiology; heart failure; L-type calcium current; calcium/calmodulin-dependent protein kinase II; late sodium current; Ion Channels/Membrane Transport

## Introduction

Heart failure (HF) is characterized by increased risk for cardiac arrhythmias. Arrhythmogenic alterations in the ventricular action potential (AP), including early and delayed afterdepolarizations,<sup>1–4</sup> AP duration (APD) prolongation,<sup>5, 6</sup> and increased beat-to-beat variability of APD<sup>6–8</sup> have been extensively studied in failing ventricular cardiomyocytes. Alterations in membrane potential stability have been associated with extensive ionic remodeling, including enhanced Na<sup>+</sup>/Ca<sup>2+</sup> exchanger current ( $I_{NCX}$ ),<sup>9, 10</sup> increased late Na<sup>+</sup> current ( $I_{NaL}$ ),<sup>11, 12</sup> and reduced repolarization reserve.<sup>13, 14</sup> In line with the electrophysiology results, the protein expression level of Na<sup>+</sup>/Ca<sup>2+</sup> exchanger (NCX) was also found to be increased in HF,<sup>9</sup> whereas that of several K<sup>+</sup> channels were decreased.<sup>15</sup> But in the case of Na<sup>+</sup> channels both the protein level and peak current density were decreased,<sup>12, 16</sup> suggesting that the increased  $I_{NaL}$  in HF results from altered regulation and gating. Accordingly, Ca<sup>2+</sup>-calmodulin-dependent protein kinase II (CaMKII), was found to be centrally involved in  $I_{NaL}$  upregulation in HF.<sup>17–19</sup>

However,  $I_{NaL}$  in previous HF studies was typically measured in non-physiologic conditions (square-pulse voltage-clamp, slow stimulation rates, strong buffering of intracellular  $Ca^{2+}$  concentration ( $[Ca^{2+}]_i$ ), and room temperature), which might have masked some important aspects of  $I_{NaL}$  regulation. Indeed,  $I_{NaL}$  was found to be larger in AP-clamped healthy guinea-pig and rabbit myocytes than the tiny  $I_{NaL}$  found in conventional voltage-clamp studies.<sup>20, 21</sup>  $\beta$ -adrenergic receptor ( $\beta$ AR) stimulation can further enhance  $I_{NaL}$  (via both CaMKII-dependent and independent mechanisms<sup>19, 21, 22</sup>) and increased sympathetic activity is commonly observed in HF. Consequently, enhanced  $I_{NaL}$  in HF may play a critical role in APD prolongation leading to cardiac arrhythmias and  $Na^+$  overload.<sup>23</sup> Accordingly, inhibition of either  $I_{NaL}$  or CaMKII was found to exert beneficial effects in HF.<sup>18, 24</sup> Unlike upregulated  $I_{NCX}$  and  $I_{NaL}$ , L-type  $Ca^{2+}$  current ( $I_{CaL}$ ) was found to be unchanged or slightly decreased in previous studies in HF.<sup>4, 25, 26</sup> However, because  $\beta$ AR signaling,  $Ca^{2+}$  and CaMKII all regulate  $I_{CaL}$ ,<sup>27–29</sup> prior voltage-clamp studies could easily misestimate changes in physiological  $I_{CaL}$  or  $I_{NaL}$  that occur during the AP in HF.

The present study measures APD,  $I_{NaL}$ ,  $I_{CaL}$  and  $I_{NCX}$  in HF versus control rabbit hearts during physiologic APs, with or without  $\beta$ AR activation and also assesses the involvement of CaMKII. We performed AP-clamp recordings with physiologic ionic composition, pacing rate,  $[Ca^{2+}]_i$  and temperature. We hypothesized that  $Ca^{2+}$  transients and increased CaMKII activity under these conditions significantly enhance inward currents in HF leading to arrhythmogenic alterations in AP morphology. We used a previously well-characterized chronic nonischemic HF rabbit model (combined volume and pressure overload), which is also arrhythmogenic.<sup>4, 9, 14, 30</sup> APs and major inward ionic currents were measured under current- and AP-clamp respectively in ventricular myocytes using specific blockers of  $I_{NaL}$  (GS-967) and  $I_{CaL}$  (nifedipine). Because under physiological conditions our nifedipine-sensitive current includes both  $I_{CaL}$  and some inward  $I_{NCX}$  (because nifedipine inhibits  $Ca^{2+}$  transients that modulate  $I_{NCX}$ ), we included computational modeling to better clarify the distinct profiles of  $I_{CaL}$  and  $I_{NCX}$  under AP-clamp. Modulation of  $I_{CaL}$  and  $I_{NaL}$  by  $Ca^{2+}$ , CaMKII, and  $\beta$ AR stimulation (ie, pathophysiological settings characteristic of HF) was also investigated to assess the regulatory changes in the net depolarizing drive during the plateau and repolarization phases of the AP.

## Methods

The data that support the findings of this study are available from the corresponding author upon reasonable request. All animal handling and laboratory procedures were in accordance with the approved protocols of the local Institutional Animal Care and Use Committee confirming to the Guide for the Care and Use of Laboratory Animals published by the US National Institute of Health (8<sup>th</sup> edition, 2011).

### Arrhythmogenic Rabbit Nonischemic HF Model

HF was induced in New Zealand White rabbits (all male, 2.5–3 kg, 3–4 months old) by aortic insufficiency and 4 weeks later by aortic constriction as previously described.<sup>9</sup> Data here was obtained from 12 HF rabbits and 8 age-matched control rabbits. HF progression was monitored periodically by echocardiography and myocytes were isolated when left

ventricular end-systolic dimension exceeded 1.4 cm (at  $\approx 2.5$  years of age). HF animals versus control hearts were near twice the heart weight/body weight ( $5.27 \pm 0.61$  versus  $2.67 \pm 0.10$  g/kg;  $P < 0.01$ ), exhibited  $\approx 40\%$  larger left ventricular end-diastolic diameter ( $2.31 \pm 0.10$  versus  $1.61 \pm 0.08$  cm;  $P < 0.001$ ),  $\approx 50\%$  larger left ventricular end-systolic diameter ( $1.63 \pm 0.08$  versus  $1.08 \pm 0.05$  cm;  $P < 0.001$ ), evidence of pulmonary congestion (lung weight,  $19.13 \pm 2.29$  versus  $14.11 \pm 0.40$  g;  $P < 0.05$ ), and abdominal ascites fluid accumulation, all similar to our prior studies on this rabbit model.<sup>4, 9, 14</sup> Enzymatic isolation of cardiomyocytes from the midmyocardial region of the left ventricular free wall was performed as previously described.<sup>14</sup>

## Electrophysiology

Isolated cells were transferred to a temperature-controlled plexiglass chamber (Cell Microsystems) and continuously superfused with a modified, bicarbonate-containing Tyrode's solution containing (in mmol/L): NaCl 124, NaHCO<sub>3</sub> 25, KCl 4, CaCl<sub>2</sub> 1.2, MgCl<sub>2</sub> 1, HEPES 10, Glucose 10, with pH=7.4. APs and underlying ionic currents were recorded in whole-cell configuration of patch-clamp technique. Electrodes were fabricated from borosilicate glass (World Precision Instruments) with tip resistances of 2 to 2.5 M $\Omega$  when filled with internal solution containing (in mmol/L): K-aspartate 110, KCl 25, NaCl 5, Mg-ATP 3, HEPES 10, cAMP 0.002, phosphocreatine-K<sub>2</sub> 10, and EGTA 0.01, with pH=7.2. This composition preserved physiological myocyte Ca<sup>2+</sup> transient and contraction.<sup>20, 31, 32</sup> Electrodes were connected to the input of an Axopatch 200B amplifier (Axon Instruments), with outputs digitized at 50 kHz using Digidata 1440A A/D card (Molecular Devices) under software control (pClamp 10). Series resistance (on cell) was typically 3 to 5 M $\Omega$  and was compensated by 85%. Experiments were discarded when the series resistance was high or increased substantially ( $>10\%$ ) during experiments. Reported AP voltages are already corrected to the liquid junction potentials. All experiments were conducted at  $37 \pm 0.1$  C.

APs were recorded in current-clamp experiments where cells were stimulated with depolarizing pulses ( $1.5 \times$  the threshold amplitude, 2 ms duration) delivered via patch pipette at pacing frequencies from 1 to 5 Hz. After reaching steady-state (3 min at each frequency), 50 consecutive APs were recorded to measure average behaviour. Then pacing was returned to 1 Hz and the selective I<sub>NaL</sub> inhibitor GS-967 (1  $\mu$ mol/L) was added to perfusate. When GS-967 effects stabilized (typically within 3 min) AP recordings at different pacing frequencies were repeated. AP duration at 95% of repolarization (APD<sub>95</sub>) was determined. Series of 50 consecutive APs were analyzed to estimate short-term variability of APD<sub>95</sub> (STV) according to the following formula:  $STV = \Sigma(|APD_{n+1} - APD_n|) / [(n_{beats} - 1) \times 2]$ , where APD<sub>*n*</sub> and APD<sub>*n+1*</sub> indicate the durations of the *n*<sup>th</sup> and (*n+1*)<sup>th</sup> APs, and *n*<sub>beats</sub> denotes the total number of consecutive beats analyzed.<sup>33</sup> Changes in STV are presented as Poincaré plots of 50 consecutive APD<sub>95</sub>.

AP-clamp experiments were conducted as previously described.<sup>14, 34, 35</sup> Briefly, the basic steps are as follows: (1) Record the cell's steady-state AP under I-clamp (self AP-clamp) or choose a previously recorded typical AP (canonical AP-clamp). (2) Apply this AP onto the cell as voltage command under V-clamp at a given pacing frequency. The net current output (reference current) should reach steady-state and be stable over time. (3) Isolate the current

of interest by using its specific blocker to remove it from the net current output (compensation current). (4) The current of interest is obtained by subtraction: Drug-sensitive current=Reference current–Compensation current. (5) Next, isolate the second current of interest by applying the second channel blocker, when it reaches steady-state another compensation current is recorded, and the second current of interest can be determined again by subtraction. Figure I in the Data Supplement shows a representative example. Under AP-clamp, all ionic currents were recorded as difference currents after each specific blocker had reached its steady-state effect (~3 min perfusion). 60 consecutive traces were recorded (to evaluate the stability) and averaged in each case before applying a drug (reference current) and 3-min after drug application (compensation current). 1  $\mu\text{mol/L}$  GS-967 and 10  $\mu\text{mol/L}$  nifedipine were used to measure  $I_{\text{NaL}}$  and  $I_{\text{CaL}}$  (including some  $I_{\text{NCX}}$ ), respectively. As previously validated,<sup>21</sup> the GS-967-sensitive current recorded in our conditions is an excellent selective measure of  $I_{\text{NaL}}$ . Experiments were performed both when  $\text{Ca}^{2+}$  cycling was preserved (Physiol) and when  $[\text{Ca}^{2+}]_i$  was buffered below the diastolic level using 10 mmol/L 1,2-bis(2-aminophenoxy)ethane-N,N,N',N'-tetraacetic acid (BAPTA) in the internal solution (BAPTA<sub>i</sub>) to assess  $[\text{Ca}^{2+}]_i$ -sensitivity of these currents under AP-clamp. To test the effect of CaMKII, cells were pretreated for 2 hours before experiment with the specific CaMKII inhibitor, autocamtide-2-related inhibitory peptide (AIP, cell-permeable myristoylated form, 1  $\mu\text{mol/L}$ ). Both the perfusion and pipettes solutions were also supplemented with AIP. In experiments examining the effect of  $\beta$ AR stimulation, isoproterenol (ISO, 3–300 nmol/L) was applied on AP-clamped cells. After ISO reached a steady-state effect ( $\approx$ 2 min), blockers were added sequentially to the perfusion solution to measure  $I_{\text{NaL}}$  and  $I_{\text{CaL}}$ . All AP-clamp experiments were performed in Tyrode solution supplemented with selective inhibitors of  $\text{K}^+$  and  $\text{Cl}^-$  currents (5 mmol/L 4-aminopyridine for  $I_{\text{to}}$ , 1  $\mu\text{mol/L}$  E-4031 for  $I_{\text{Kr}}$ , 1  $\mu\text{mol/L}$  HMR-1556 for  $I_{\text{Ks}}$ , 300  $\mu\text{mol/L}$   $\text{BaCl}_2$  for  $I_{\text{K1}}$ , 100 nmol/L apamin for  $I_{\text{KCa}}$ , and 30  $\mu\text{mol/L}$  CaCCinh-A01 for  $I_{\text{ClCa}}$ ). Experiments were excluded from analysis if significant rundown of  $I_{\text{CaL}}$  was observed (in periodic tests) or if membrane current did not reach steady-state.

Conventional square pulse voltage-clamp experiments to measure the biophysical parameters of  $I_{\text{CaL}}$  was performed using pipette solution containing 5 mmol/L EGTA and 2.1 mmol/L  $\text{CaCl}_2$  (free  $[\text{Ca}^{2+}]_i=100$  nmol/L using the MaxChelator software), and in the presence of selective  $\text{K}^+$  and  $\text{Cl}^-$  channel inhibitors in the bath (as above) and  $\text{Na}^+$  was replaced by  $\text{Li}^+$  to inhibit NCX.  $I_{\text{CaL}}$  was measured using a 500 ms long voltage steps from holding potential of  $-80$  mV to test potentials (between  $-40$  and  $+20$  mV) every 5 s (0.2 Hz stimulation) with a 50-ms pre-step to  $-40$  mV to inactivate  $\text{Na}^+$  channels. To investigate  $\text{Ca}^{2+}$ /CaMKII-dependence of  $I_{\text{CaL}}$ , a 100-ms long depolarization pulse to 0 mV were used in every 0.5 s (2 Hz stimulation).

Ion currents were normalized to cell capacitance, determined in each cell using short (10 ms) hyperpolarizing pulses from  $-10$  mV to  $-20$  mV. Cell capacitance was  $144.4\pm 1.2$  pF in age-matched controls (118 cells/8 animals) versus  $194.1\pm 3.3$  pF in HF (158 cells/12 animals) using 2-sample Student's *t* test,  $P<0.001$ .

Chemicals and reagents were purchased from Sigma-Aldrich, if not specified otherwise. E-4031 and HMR-1556 were from Tocris Bioscience. GS-967 was from Gilead.

## Computational Modeling and Simulation

*In silico* experiments were performed using our recently updated rabbit ventricular myocyte model<sup>36</sup> that integrates detailed descriptions of membrane electrophysiology, Ca<sup>2+</sup> and Na<sup>+</sup> handling,<sup>37</sup> protein kinase A and CaMKII signalling pathways,<sup>38</sup> and myofilament contraction.<sup>39</sup> This model describes changes in CaMKII activity during each heartbeat, resulting in dynamic functional modulation of CaMKII phosphorylation targets (L-type Ca<sup>2+</sup> channels, ryanodine receptors and phospholamban). These effects are enhanced in HF, where CaMKII expression and activation is increased (and as in prior work we elevated CaMKII content to 6-fold).<sup>38</sup> We updated our model to account for HF-induced remodeling, based on our new data here and our previous HF model (including two-fold increase in NCX maximal transport rate, and altered sarcoplasmic reticulum (SR) Ca<sup>2+</sup> release and reuptake).<sup>40</sup> Based on our novel I<sub>CaL</sub> observations here, we shifted steady-state activation (5 mV negative) but left steady-state inactivation unchanged in HF. We also reduced I<sub>CaL</sub> maximal conductance (G<sub>CaL</sub>) by 20% in HF, resulting in the unaltered peak I<sub>CaL</sub> that we observed in control versus HF myocytes (Table and Figure II in the Data Supplement).

We used our updated cellular models to simulate AP-clamp experiments at 2 Hz pacing in control and HF myocytes with physiologic Ca<sup>2+</sup> handling (Figure III in the Data Supplement; exhibiting reduced Ca<sup>2+</sup> transients in HF) and/or with CaMKII inhibition (simulated by clamping fractional phosphorylation of CaMKII targets to the levels predicted without pacing). We applied the same AP trace used in wet AP-clamp experiments as the voltage-command. All simulations were performed in MATLAB (The MathWorks, Natick, MA, USA) using the stiff ordinary differential equation solver *ode15s*. Model code is available for download at: <https://somapp.ucdmc.ucdavis.edu/Pharmacology/bers/> or <http://elegrandi.wixsite.com/grandilab/downloads>.

## Statistical Analysis

Data are presented as Mean±SEM. The number of cells in each experimental group was reported as *n*=number of cells/number of animals. Statistical significance of differences was tested by paired Student's *t* test or analysis of variance (ANOVA) with Bonferroni posttest as appropriate using Origin2016 software. Differences were deemed significant if *P*<0.05.

## RESULTS

### Frequency-Dependent Changes in AP Shape and Effect of Late Na<sup>+</sup> Current Inhibition in HF

Figure 1 shows representative APs and group analysis in HF and age-matched control myocytes before and after treatment with the selective I<sub>NaL</sub> inhibitor GS-967 (1 μM). Baseline APD at 95% repolarization (APD<sub>95</sub>) was longer in HF versus control at 1 Hz pacing (269.5±17.5 versus 199.2±7.7 ms; *P*<0.001) (Figure 1A and 1B). GS-967 decreased APD<sub>95</sub> in HF by 22% (to 211.6±6.8 ms, *NS*), and also decreased APD<sub>95</sub> in control, but by only 13% (to 174.2±5.9 ms; *P*<0.001). At faster pacing rates APD<sub>95</sub> converged for HF and control, and similarly for the +GS-967 treatment curves (Figure 1B). Resting membrane potential (RMP) was slightly depolarized (by ≈4 mV, Figure 1C) in HF consistent with reduced I<sub>K1</sub> in HF.<sup>4, 5, 14</sup> AP amplitude (APA) was significantly lower (by 8–10 mV) in HF

independent of GS-967 treatment. Similarly, the maximum rate of rise ( $dV/dt_{max}$ ) during AP upstroke was also decreased by  $\approx 25\%$  in HF (Figure 1D). These effects are likely to be at least partly attributed to lower  $Na^+$  channel availability (with the more positive diastolic  $V_m$ ), but elevated intracellular  $[Na^+]$  ( $[Na^+]_i$ ) and altered  $Na^+$  channel expression (both known to occur in HF)<sup>41–43</sup> could also be involved. These effects were similar upon acute  $I_{NaL}$  inhibition with GS-967. The maximum repolarization rate ( $-dV/dt_{max}$ ) during AP phase 3 was significantly slower in HF (by  $\approx 25\%$ ), and  $I_{NaL}$  block partially restored  $-dV/dt_{max}$  and limited the difference between control and HF ( $\approx 15\%$ ). Collectively, these data are consistent with peak  $I_{Na}$  amplitude in HF being normal except for slight reduction in availability associated with the slightly depolarized diastolic  $V_m$ , and smaller APA and  $dV/dt_{max}$ , but enhanced  $I_{NaL}$  that contributes to APD prolongation and slowed repolarization.

Figure 1E and 1F show that HF myocytes also exhibited higher short-term variability of  $APD_{95}$  (STV) at 1 and 2 Hz, in HF versus control ( $4.80 \pm 0.51$  versus  $3.21 \pm 0.21$  ms, respectively, 1 Hz pacing;  $P < 0.01$ ). Importantly, GS-967 treatment in HF decreased not only mean  $APD_{95}$  but also STV to control values ( $3.19 \pm 0.46$  ms; *NS*). GS-967 also decreased STV at all pacing rates in control ( $2.10 \pm 0.13$  ms;  $P < 0.001$ ).

### $I_{NaL}$ Magnitude and Dynamics Changes Under AP in HF

The AP data indicate increased depolarization drive during the AP plateau and repolarization phases in HF versus control myocytes. Thus, we studied the 3 major inward plateau currents ( $I_{NaL}$ ,  $I_{CaL}$ , and  $I_{NCX}$ ) under physiological AP-clamp. We did not measure the fast  $Na^+$  current due to technical limitations (peak  $I_{Na}$  overlaps the capacitive transient under physiological AP-clamp), but altered peak  $I_{Na}$  can contribute to pathological excitability in HF.<sup>44</sup> The reduced  $dV/dt_{max}$  observed (Figure 1D) would be consistent with reduced  $Na^+$  current availability and peak  $I_{Na}$  in HF. GS-967-sensitive  $I_{NaL}$  and nifedipine-sensitive current were recorded from the same myocyte using AP-clamp sequential dissection<sup>21, 35</sup> (Figure I in the Data Supplement) with either preserved  $[Ca^{2+}]_i$  cycling (Physiol) or with  $[Ca^{2+}]_i$  buffered with 10 mmol/L BAPTA in the pipette (BAPTA<sub>i</sub>). Involvement of CaMKII was also tested using the selective CaMKII inhibitory peptide AIP. A previously recorded typical rabbit ventricular AP was used as voltage command in all AP-clamp experiments (ie, a canonical AP-clamp analogous to the mean for 2 Hz where HF and control  $APD_{95}$  were similar).<sup>14</sup> Because HF myocytes were larger ( $\approx 35\%$  increase in cell capacitance) all reported currents are normalized to the corresponding cell capacitance.

$I_{NaL}$  was measured as GS-967-sensitive current under AP-clamp (Figure 2; See Reference 21 and Figure 1 therein for additional controls and technical details).<sup>21</sup> The density of  $I_{NaL}$  increased during AP repolarization as the driving force for  $Na^+$  influx increased, achieving peak density during phase 3 repolarization of the AP (at  $\approx -50$  mV in both control and HF). Importantly, peak  $I_{NaL}$  density was 82% higher in HF versus control myocytes in our physiological condition ( $-0.93 \pm 0.03$  versus  $-0.51 \pm 0.01$  A/F, respectively;  $P < 0.001$ ; Figure 2A and 2D). The  $I_{NaL}$  I-V analysis reveals that  $I_{NaL}$  is increased during the entire AP without change in  $V_m$ -dependence (Figure 2A, bottom). Buffering  $[Ca^{2+}]_i$  with BAPTA<sub>i</sub> did not alter peak  $I_{NaL}$  density in control ( $-0.54 \pm 0.02$  A/F; *NS*; Figure 2E), but decreased peak

$I_{\text{NaL}}$  by 23% in HF ( $-0.72 \pm 0.03$  A/F;  $P < 0.001$ ; Figure 2B). Nevertheless,  $I_{\text{NaL}}$  density and integral charge were still larger in HF versus control myocytes with BAPTA<sub>i</sub> (Figure 2E and 2F). AIP pretreatment (to inhibit CaMKII) decreased  $I_{\text{NaL}}$  in HF to the level of untreated control ( $-0.54 \pm 0.02$  A/F; NS; Figure 2C and 2D). However, AIP also decreased  $I_{\text{NaL}}$  in control ( $-0.37 \pm 0.01$  A/F;  $P < 0.001$ ; Figure 2C and 2D), such that  $I_{\text{NaL}}$  was still higher in HF versus control after AIP treatment (as for BAPTA<sub>i</sub>). We conclude that  $I_{\text{NaL}}$  is elevated in HF under all conditions studied, that basal  $I_{\text{NaL}}$  at 2 Hz pacing with Ca<sup>2+</sup> transients, is partly dependent upon CaMKII activity, and that large  $I_{\text{NaL}}$  increase in HF is substantially CaMKII-dependent.

We used this data to update our most recent computational model of the rabbit ventricular myocyte.<sup>36</sup> The basal value of  $I_{\text{NaL}}$  maximal conductance ( $G_{\text{NaL}}$ ) was scaled to 0.0527 mS/μF to reflect the peak  $I_{\text{NaL}}$  observed during the AP in control myocytes with physiologic Ca<sup>2+</sup> handling. Inactivation of  $I_{\text{NaL}}$  was set to 600 ms as previously.<sup>45</sup>  $G_{\text{NaL}}$  was modeled as a function of chronic HF-induced remodeling (not influenced by acute CaMKII inhibition, ie, 50% increase in  $G_{\text{NaL}}$  in failing versus nonfailing myocytes -guided by data in AIP-treated cells, Figure 2C) and simulated CaMKII activation reproduced the increase in peak  $I_{\text{NaL}}$  observed with physiologic Ca<sup>2+</sup> handling versus CaMKII inhibition in both failing and nonfailing conditions, as previously done.<sup>46</sup>  $G_{\text{NaL}}$  (in mS/μF) was calculated as:

$$G_{\text{NaL}} = 0.0527 \cdot \left(1 + 0.5 \cdot \text{HF}_{\text{remodeling}}\right) \cdot \frac{1.27}{1 + e^{\frac{(P_{\text{NaVs}} - 0.12)}{0.1}}}$$

where  $\text{HF}_{\text{remodeling}}$  indicates the absence/presence of chronic HF-induced remodeling (0 and 1, respectively), and  $P_{\text{NaVs}}$  (ranging from 0 to 1) is the fraction of phosphorylated Na<sup>+</sup> channels, modeled as previously described (Figure IV in the Data Supplement).<sup>46</sup> The *in silico* AP-clamp experiments quantitatively reproduced the experimental data on the role of physiological Ca<sup>2+</sup> transients and CaMKII activity in upregulating  $I_{\text{NaL}}$  in control and more strongly in HF (Figure 2G through 2I).

### Nifedipine-sensitive Inward Current Changes in HF ( $I_{\text{CaL}}$ and $I_{\text{NCX}}$ )

Next, we measured nifedipine-sensitive current ( $I_{\text{Nife}}$ ) under AP-clamp (Figure 3). Under physiological conditions, nifedipine inhibits  $I_{\text{CaL}}$ , and consequently abolishes Ca<sup>2+</sup> transients. Note that  $I_{\text{Nife}}$  was recorded when other Ca-sensitive currents (eg,  $I_{\text{Ks}}$ ,  $I_{\text{K(Ca)}}$  and  $I_{\text{Cl(Ca)}}$ ) were pharmacologically inhibited (see Methods). Thus, the measured  $I_{\text{Nife}}$  is a composite current containing  $I_{\text{CaL}}$  and the inward shift in  $I_{\text{NCX}}$  that is driven by elevated  $[\text{Ca}]_i$ . Peak  $I_{\text{Nife}}$  density in the early plateau phase of the AP (at  $\approx +35$  mV in both control and HF) was unaltered in HF versus control under physiological condition (Figure 3A and 3D). However,  $I_{\text{Nife}}$  was slightly increased in HF during the AP plateau and terminal repolarization phases (Figure 3A and 3E), potentially due to either less Ca<sup>2+</sup>-dependent inactivation (CDI) of  $I_{\text{CaL}}$  in HF (due to reduced Ca<sup>2+</sup> transients)<sup>4, 9</sup>, enhanced Ca<sup>2+</sup>/CaMKII-dependent facilitation (CDF), altered Ca<sup>2+</sup> channel subunit composition, or alternatively, but less likely<sup>41</sup> to more inward  $I_{\text{NCX}}$ . In contrast, when  $I_{\text{Nife}}$  was recorded with BAPTA<sub>i</sub> (ie, without Ca<sup>2+</sup> transient and inward  $I_{\text{NCX}}$ ), peak  $I_{\text{Nife}}$  density (more

exclusively  $I_{CaL}$ ) under AP-clamp was significantly decreased in HF (Figure 3B and 3D), but BAPTA also abolished the small hump near terminal repolarization, consistent with loss of expected inward  $I_{NCX}$  at this time (note superimposition of  $I_{Nife}$  versus  $V_m$  curve between  $-80$  and  $-40$  mV). In BAPTA<sub>i</sub> the  $I_{Nife}$  decay was still slower in HF versus control, despite low CDI expected in both cases (Figure 3B and 3E). When CaMKII was inhibited, the  $I_{Nife}$  density and integrated charge movement were reduced versus Physiol for both HF and control (Figure 3C, 3D, and 3F). Since the peak inward  $I_{Nife}$  is likely dominated by peak  $I_{CaL}$ , this might reflect the involvement of basal CaMKII activity in maintaining physiological peak  $I_{CaL}$  when  $Ca^{2+}$  transients and CaMKII are functional (Figure 3A and 3D).

### Changes in the Biophysical Properties of L-type $Ca^{2+}$ Current in HF

Next, we measured the biophysical parameters of  $I_{CaL}$  using conventional square-pulse voltage-clamp and  $[Ca^{2+}]_i$  buffered to 100 nmol/L by inclusion of 5 mmol/L EGTA in the pipette solution. The peak density of  $I_{CaL}$  and the I-V relationship were not significantly different (Figure 4A), but the steady-state activation curve of  $I_{CaL}$  was shifted slightly (4.7 mV) to more negative potentials in HF versus control (Figure 4B). The inactivation time constants of  $I_{CaL}$  (obtained by biexponential fits of  $I_{CaL}$  decay) were slightly prolonged in HF versus control, consistent with slower CDI in HF (Figure 4D and 4E), but  $V_m$ -dependence of inactivation (Figure 4C) and the recovery from inactivation kinetics (Figure 4F) were unchanged.

We also analyzed  $I_{CaL}$  in the pipette conditions used for AP-clamp studies (Physiol, BAPTA<sub>i</sub>, and CaMKII inhibition). Peak  $I_{CaL}$  density elicited by a step pulse to 0 mV was unaltered in HF versus control with preserved  $[Ca^{2+}]_i$  cycling (Figure 4G). This contrasts with the diminished peak  $I_{CaL}$  observed when either  $[Ca^{2+}]_i$  is clamped very low (BAPTA<sub>i</sub>) or CaMKII is inhibited (Figure 4H and 4I), both conditions where CaMKII-dependent CDF is suppressed. We infer that  $Ca^{2+}$ -dependent CaMKII upregulates peak  $I_{CaL}$  (via CDF) in HF to the level of control cells (when measured in physiological conditions; compare Figure 4G through 4I).

CDI of  $I_{CaL}$  was, as expected, stronger under physiological  $[Ca^{2+}]_i$  versus when  $[Ca^{2+}]_i$  was buffered by EGTA or BAPTA (Figure 4G versus 4E and 4H). However, the  $\tau$  of inactivation was significantly slowed in HF versus control (Figure 4G, inset), consistent with known smaller  $Ca^{2+}$  transients in HF and thus less CDI.<sup>4,9</sup> Using 10 mmol/L BAPTA in the pipette (BAPTA<sub>i</sub>) should eliminate both CDI as well as CDF (Figure 4H). Indeed, BAPTA<sub>i</sub> significantly slowed the  $\tau$  of inactivation (versus Physiol or EGTA; Figure 4H and 4I) but  $\tau_{fast}$  was still slightly slower in HF versus control (Figure 4H, inset). When CaMKII was inhibited with AIP (Figure 4I) the inactivation  $\tau$  values were more like those in physiological buffer (Figure 4G). The slowed  $I_{CaL}$  inactivation in HF was still observable in BAPTA, consistent with part of that effect being independent of CDI, and may reflect some PKA-dependent effect in HF myocytes.<sup>47, 48</sup>

## Computer Models Help to Report Physiological $I_{CaL}$ and $I_{NCX}$ during the AP in HF

To help delineate the relative contributions of  $I_{CaL}$  and  $I_{NCX}$  to  $I_{Nife}$  under AP-clamp, we used our rabbit ventricular myocyte model<sup>36</sup> with  $I_{CaL}$  properties tuned to those measured in Figure 4 (for details see Methods, Table and Figure II in the Data Supplement). Figure 5 shows how *in silico* experiments can inform the distinct profiles of  $I_{CaL}$  and  $I_{NCX}$  under AP-clamp in control and HF cells under physiologic  $Ca^{2+}$  transients (Figure III in the Data Supplement). Figure 5A and 5B shows calculated  $I_{CaL}$  and  $I_{Na/Ca}$  in physiological conditions, which have the expected overall shapes.<sup>10, 37, 41, 49, 50</sup> After  $I_{CaL}$  activation and the start of SR  $Ca^{2+}$  release, CDI causes  $I_{CaL}$  decline to a plateau that can increase slightly as AP repolarization causes an increase in the  $Ca^{2+}$  driving force, until terminal repolarization deactivates  $I_{CaL}$ .  $I_{NCX}$  is initially outward ( $Ca^{2+}$  influx) driven by the rapid AP depolarization. But once SR  $Ca^{2+}$  release occurs, the high submembrane  $[Ca^{2+}]_i$  drives a first peak of inward  $I_{NCX}$  which declines as  $[Ca^{2+}]_i$  falls, but is followed by a second peak during terminal repolarization (driven by voltage) until the  $[Ca^{2+}]_i$  reaches the diastolic level. In HF the  $I_{CaL}$  waveform is similar, although CDI is slowed. The higher  $[Na^+]_i$  and smaller  $Ca^{2+}$  transient in HF shifts the  $I_{NCX}$  waveform outward during the plateau, and the higher NCX expression levels cause the larger inward  $I_{NCX}$  tail upon final repolarization.<sup>10, 41</sup>

Figure 5C and 5D shows how  $I_{CaL}$  and  $I_{NCX}$  are expected to change following 3-min of nifedipine exposure, which blocks  $I_{CaL}$  and SR  $Ca^{2+}$  release. Without  $I_{CaL}$  or SR  $Ca^{2+}$  release the AP drives outward  $I_{NCX}$  ( $Ca^{2+}$  influx) throughout much of the AP, and then that same amount of  $Ca^{2+}$  which entered via outward  $I_{NCX}$  is extruded via inward  $I_{NCX}$  during repolarization. Higher NCX expression in HF myocytes makes inward and outward  $I_{NCX}$  larger in HF. The residual  $I_{NCX}$  during nifedipine exposure must be taken into account when inferring the predicted  $I_{Nife}$  shown in Figure 5E and 5F. The shape of the predicted  $I_{Nife}$  is similar to the  $I_{Nife}$  recorded *in vitro* under AP-clamp in cardiomyocytes (Figure 3A). This analysis also explains why the inward  $I_{NCX}$  tail at terminal repolarization is less prominent than expected in the measured  $I_{Nife}$  traces in Figure 3A and 3C. While this simulation analysis cannot extract absolute  $I_{CaL}$  and  $I_{NCX}$  waveforms that occur during the AP in control versus HF myocytes, Figure 5A provides a qualitative estimate of likely changes that occur in  $I_{CaL}$  and  $I_{NCX}$  during the HF AP.

## Altered $\beta$ -Adrenergic Response of Inward Currents in HF

Elevated sympathetic tone is often reported in HF in conjunction with altered responses to  $\beta$ AR activation. We therefore tested the effects of acute  $\beta$ AR stimulation on  $I_{NaL}$  and  $I_{Nife}$  in HF versus control myocytes using AP-clamp. Because downstream effects of  $\beta$ AR stimulation are mediated both by protein kinase A (PKA) and CaMKII and the activities of these kinases are known to be altered in HF, ionic currents were measured again with physiological preserved  $[Ca^{2+}]_i$  cycling and with heavily buffered  $[Ca^{2+}]_i$ .

Figure 6A shows  $I_{NaL}$  measured after  $\beta$ AR agonist isoproterenol (ISO, 10 nM) treatment. ISO increased  $I_{NaL}$  in both control and HF myocytes, but by a much larger percent in control (by 110% versus 40%; Figure 6C). Nevertheless, the resulting  $I_{NaL}$  with ISO (and its integral) was still larger in HF. Buffering  $[Ca^{2+}]_i$  reduced the effect of ISO on  $I_{NaL}$ ,

indicating the involvement of  $\text{Ca}^{2+}$  and/or CaMKII (as well as PKA) in mediating the ISO effect. Again, the effect on control was larger than in HF (70% versus 30%). Moreover, in BAPTA<sub>i</sub> the ISO-induced  $I_{\text{NaL}}$  peak density was not significantly different between control and HF. That is consistent with  $\text{Ca}^{2+}$ - or CaMKII-dependence being involved with ISO-induced higher  $I_{\text{NaL}}$  in HF versus control.

$I_{\text{Nife}}$  also increased after ISO treatment, as expected for the known effects of  $\beta$ AR stimulation on  $I_{\text{CaL}}$  and  $\text{Ca}^{2+}$  transient amplitude (which drives inward  $I_{\text{NCX}}$ ; Figure 6B). Again, the ISO-induced increase in  $I_{\text{Nife}}$  was smaller in HF. This blunted  $\beta$ AR response in HF was present with both physiological  $\text{Ca}^{2+}$  cycling and BAPTA<sub>i</sub> conditions, but for  $I_{\text{Nife}}$  the ISO-induced increase for BAPTA<sub>i</sub> (2.4-fold in control versus 2-fold in HF) was only slightly smaller than for physiological conditions (3.3-fold in control versus 2.2-fold increase in HF; Figure 6D).

Because the ISO effects on both  $I_{\text{NaL}}$  and  $I_{\text{Nife}}$  were blunted in HF versus control, we tested whether this was due to decreased ISO-sensitivity or limited maximal response. ISO concentrations between 3 and 300 nM were applied in HF and control (Figure 7). Steady-state contracting AP-clamped myocytes in HF were unstable at higher ISO concentrations, so these experiments were performed with 10 mmol/L BAPTA in the pipette (BAPTA<sub>i</sub>). ISO increased  $I_{\text{NaL}}$  in both control and HF, but the half maximal [ISO] ( $\text{EC}_{50}$ ) was slightly higher in HF ( $16.1 \pm 1.4$  versus  $10.5 \pm 1.3$  nM;  $P < 0.05$ ; Figure 7A). However, the maximal ISO-induced  $I_{\text{NaL}}$  density was not different in control versus HF (Figure 7A).  $I_{\text{CaL}}$  was also markedly increased after ISO application with similar  $\text{EC}_{50}$  ( $\approx 12$  nM) in control and HF. However, the maximal  $I_{\text{CaL}}$  response after ISO stimulation was only half as much in HF versus control (4.6- versus 2.7-fold increase in peak  $I_{\text{CaL}}$ ; Figure 7B). This indicates unchanged ISO-sensitivity, but weaker potency in raising  $I_{\text{CaL}}$ . The blunted ISO response of  $I_{\text{CaL}}$  in HF may limit  $\text{Ca}^{2+}$  transients and inotropy in HF during sympathetic activity.

### Relative Contributions of Inward Currents to AP Plateau and Phase 3 Repolarization

The dynamic interplay of time- and voltage-dependent activation and inactivation of inward currents governs the AP waveform. Each inward current has a unique profile and magnitude during the cardiac AP. The relative contributions of major inward currents ( $I_{\text{NaL}}$ ,  $I_{\text{Nife}} \approx I_{\text{CaL}} + I_{\text{NCX}}$ ) during the AP plateau and repolarization in control and in HF are shown in Figure 8, compared at different  $V_m$  (+40, -20, and -60 mV), and shown as integrated charge movement during the AP (Figure 8, insets).  $I_{\text{Nife}}$  early in the AP (phase 1, at +40 mV) predominantly represents  $I_{\text{CaL}}$ , whereas late during terminal repolarization (at -60 mV) is mainly inward  $I_{\text{NCX}}$  (during physiological  $\text{Ca}^{2+}$  transients).

Total inward current during AP phase 1 (early repolarization) was unaltered in HF versus control in physiologic conditions, but had greater  $I_{\text{NaL}}$  contribution in HF (Figure 8A and 8B). Later during AP repolarization (-20 and -60 mV) total inward current was higher in HF, mainly due to increased  $I_{\text{NaL}}$  (Figure 8B). In control myocytes, ISO increased both inward currents, but the smaller ISO-induced increases of  $I_{\text{CaL}}$  in HF reduced  $I_{\text{CaL}}$  throughout the AP (Figure 8C). Total inward current in HF was reduced early (+40 mV) but increased progressively later in the AP (-20 and -60 mV) which could promote failure of

repolarization and EADs. Despite  $\beta$ AR hyporesponsiveness,  $I_{NaL}$  and  $I_{NCX}$  were still higher in HF and contributed to that increased total inward current late in the AP (with ISO).

In contrast to physiological conditions, CaMKII inhibition limited both  $I_{NaL}$  and  $I_{Nife}$  increases in HF and abolished differences in late AP total inward current between HF and control (Figure 8D versus 8B). Similarly, using strong  $[Ca^{2+}]_i$  buffering also reduced  $I_{NaL}$  and  $I_{Nife}$  in HF, and total inward current was unaltered early but still slightly increased late during the AP in HF versus control (Figure 8E). ISO did not change total inward current during phase 3 of the AP in the presence of BAPTA<sub>i</sub> (presumably because inward  $I_{NCX}$  is prevented; Figure 8F).

## Discussion

### Arrhythmogenic AP Alterations in HF and the Role of Increased Late Na<sup>+</sup> Current

HF-induced ionic remodeling causes characteristic changes in ventricular AP profile in our rabbit HF model including APD prolongation, reduction of phase 1 and phase 3 repolarization rates, depolarized resting membrane potential and reduced AP upstroke velocity under steady-state pacing (see Figure 1A through 1D), which mostly agree with literature data on various animal HF models and human HF.<sup>4–7, 18, 25, 26, 51</sup> Moreover, temporal variability of AP repolarization (characterized by STV) was also increased in HF (Figure 1E and 1F), further enhancing the arrhythmogenic substrate.<sup>6–8</sup> Delayed afterdepolarizations are frequently reported in HF,<sup>3, 4</sup> and we have shown previously increased DADs that depended on CaMKII-mediated SR Ca<sup>2+</sup> leak after cessation of pacing bouts in this HF model.<sup>14, 52, 53</sup>

The HF-related arrhythmogenic alterations in ventricular AP were more pronounced at slow pacing rates than at fast pacing rates (Figure 1) in line with previous experimental<sup>14, 54</sup> and clinical data.<sup>55</sup> Importantly, selective  $I_{NaL}$  inhibition in HF reduced both APD and STV to control values at all pacing rates. The rate-dependence of APD prolongation and increase in STV associated with enhanced  $I_{NaL}$  in HF can be explained by the following mechanisms: (1)  $I_{NaL}$  availability may decrease at faster pacing rates.<sup>56</sup> (2) Amplitude of Ca<sup>2+</sup> transients may decrease at faster pacing rates in HF cells unlike healthy control, altering the magnitude of Ca<sup>2+</sup>-dependent ionic currents and  $I_{NCX}$ .<sup>57</sup> (3) The delayed rectifier K<sup>+</sup> currents that counterbalance  $I_{NaL}$  during AP plateau and phase 3 are also increased in HF under physiological conditions at faster pacing rates,<sup>14</sup> and the increase of those K<sup>+</sup> currents has also been shown to be Ca<sup>2+</sup>/CaMKII-dependent.<sup>14</sup>

In line with our results in HF rabbits, it has been shown that both the  $I_{NaL}$  inhibitor ranolazine and AIP exert potent antiarrhythmic effects in a transverse aortic constriction (pressure overload) induced HF model in mice<sup>18</sup> as well as in failing human myocytes.<sup>24</sup> Inhibition of the enhanced  $I_{NaL}$  prevented APD prolongation and STV enhancement in our rabbit HF model, thus it reduced the substrate for arrhythmias. Moreover, enhanced  $I_{NaL}$  can also contribute to increased Na<sup>+</sup> loading and (via NCX) Ca<sup>2+</sup> loading, and contribute to increased occurrence of afterdepolarizations that triggers arrhythmias in HF.<sup>23</sup> Furthermore, enhanced Na<sup>+</sup> current and spontaneous SR Ca<sup>2+</sup> leak can contribute to increased STV.<sup>33, 58</sup> Of note, the  $I_{NaL}$  maximal conductance used in the mathematical model to fit our AP-clamp

current data is ~10-fold larger than previously estimated in rabbit myocyte experiments using a different experimental approach (1-day cell culture, square voltage pulses to  $-20$  mV, abolished  $\text{Ca}^{2+}$  cycling).<sup>45</sup> Physiologically dynamic  $\text{Ca}^{2+}$ -dependent CaMKII activation and AP shape may contribute to these differences which underlines the importance of using physiological AP-clamp to measure ionic currents.

### Changes in Inward Currents in HF that Shape the AP

Electrophysiological remodeling in HF leads to arrhythmogenic alterations in AP morphology that involves changes in the expression and regulation of multiple ion channels.<sup>26</sup> Experimental data detailing such changes have been integrated in computational models to understand mechanistically how arrhythmogenesis occurs in HF.<sup>40, 59</sup> However, ionic currents were usually recorded under nonphysiologic conditions, which may mask modulation by  $\text{Ca}^{2+}$  transients and CaMKII on ionic currents. This regulation may be even more impactful under pathological states including HF (where CaMKII-activity is increased).<sup>14, 52, 60</sup> Accordingly, we have shown that  $\text{Ca}^{2+}$  transient, CaMKII, and  $\beta\text{AR}$  stimulation regulates  $\text{K}^+$  currents under physiological AP-clamp, and importantly, that this regulation was significantly altered in HF.<sup>14</sup> Importantly,  $\text{Ca}^{2+}/\text{CaM}$  and CaMKII are also known to regulate both  $\text{Na}^+$  and  $\text{Ca}^{2+}$  channels.  $\text{Ca}^{2+}/\text{CaM}$  binding to the IQ motif of these channels is known to enhance CDI that is evident, especially for  $\text{I}_{\text{CaL}}$ ,<sup>61, 62</sup> but a similar mechanism has been shown for fast  $\text{I}_{\text{Na}}$  and  $\text{I}_{\text{NaL}}$ .<sup>63, 64</sup> CDI serves as a feedback mechanism preventing cellular  $\text{Ca}^{2+}$  overload.<sup>29</sup> In contrast, CaMKII increases both  $\text{I}_{\text{CaL}}$  (via CDF)<sup>27–29</sup> and  $\text{I}_{\text{NaL}}$ .<sup>17, 64</sup>

$\text{I}_{\text{NaL}}$  represents a non- or slowly-inactivating component of  $\text{Na}^+$  current that persists throughout the AP plateau and phase 3, as shown in Figure 2. The gating mechanism(s) contributing to  $\text{I}_{\text{NaL}}$  have been extensively studied and may include the early burst and late scattered openings, non-equilibrium gating and steady-state “window” current (overlap between the activation and inactivation curves); however, the details are still not fully resolved.<sup>65</sup>  $\text{I}_{\text{NaL}}$  enhancement in HF has been demonstrated in different animal models and human;<sup>11, 12</sup> however, we found an even more pronounced increase in  $\text{I}_{\text{NaL}}$  under physiological AP-clamp than previous reports of smaller  $\text{I}_{\text{NaL}}$  under nonphysiological voltage-clamp conditions.<sup>11, 17, 19, 45, 56</sup> We showed that  $\text{I}_{\text{NaL}}$  upregulation in HF was largely  $\text{Ca}^{2+}$ -dependent (Figure 2), in line with the increased CaMKII activity in HF that upregulates  $\text{I}_{\text{NaL}}$ .<sup>17–19</sup> However,  $\text{I}_{\text{NaL}}$  was still increased in HF following cytosolic  $\text{Ca}^{2+}$  buffering with BAPTA, potentially reflecting an increased basal PKA-dependent phosphorylation of  $\text{Na}^+$  channels or remodeling with increased expression of neural  $\text{Na}^+$  channel isoforms in HF.<sup>42, 43</sup>

$\text{I}_{\text{CaL}}$  is the main inward current during the AP plateau in ventricular cardiomyocytes, as shown in Figure 3.  $\text{I}_{\text{CaL}}$  amplitude was unchanged in HF under physiological conditions or using the slow  $\text{Ca}^{2+}$  buffer EGTA (which does not eliminate subsarcolemmal  $[\text{Ca}^{2+}]$  changes, Figure 4). In contrast,  $\text{I}_{\text{CaL}}$  was slightly decreased in HF when measured with BAPTA<sub>i</sub> and AIP, indicating a key role of CaMKII in maintaining  $\text{I}_{\text{CaL}}$  in HF.  $\text{I}_{\text{CaL}}$  decay was significantly slower in HF. This might be explained by reduced CDI (because of reduced  $\text{Ca}^{2+}$  transient amplitude), enhanced CDF (via increased CaMKII activity), and/or

altered  $\text{Ca}^{2+}$  channel subunit composition. Increased expression of auxiliary  $\beta_2$  subunit is known to occur in HF<sup>66</sup> and it has been shown to reduce the rate of  $I_{\text{CaL}}$  inactivation, shift activation to more negative potentials, and significantly diminishes PKA response, all in agreement with our data.<sup>67–69</sup>

The difference in nifedipine-sensitive inward current measured with and without  $[\text{Ca}^{2+}]_i$  buffering suggests enhanced  $I_{\text{NCX}}$ , in agreement with previous reports.<sup>9</sup>  $I_{\text{NCX}}$  kinetics during the rabbit ventricular AP during  $\text{Ca}^{2+}$  transients was previously measured in an elegant study of Weber et al.<sup>49</sup> Here, we could not explicitly separate  $I_{\text{NCX}}$  from  $I_{\text{Nife}}$  (Figure 3), but our measurements of  $I_{\text{CaL}}$  alone (Figure 4) and *in silico* models (Figure 5) were consistent with the upregulation of NCX previously reported in this HF model. Our modeling provided quantitative estimates of  $I_{\text{NCX}}$  dynamics under AP-clamp in control and HF (Figure 5). Importantly, the increased  $I_{\text{NCX}}$  peak during phase 3 of AP repolarization in HF may contribute to EADs and APD prolongation. However, the precise contribution of  $I_{\text{NCX}}$  to arrhythmogenic AP alterations in HF requires further studies.

### **$\beta$ -Adrenergic Stimulation-Induced Changes in Inward Currents in HF**

Increased sympathetic activity but blunted  $\beta$ -adrenergic response are hallmarks of HF and significantly contribute to contractile dysfunction, alterations in  $\text{Ca}^{2+}$  handling system, and arrhythmogenesis.<sup>4, 14, 52, 70, 71</sup>

$I_{\text{CaL}}$ ,  $I_{\text{NaL}}$ , and  $I_{\text{NCX}}$  are all known to be increased in ventricular myocytes after  $\beta\text{AR}$  stimulation. Downstream signaling mediating  $\beta\text{AR}$  effects on  $\text{Na}^+$  and  $\text{Ca}^{2+}$  channels involves both PKA and CaMKII; however, there is still debate on the exact molecular mechanisms and phosphorylation sites.<sup>72, 73</sup> We found that  $I_{\text{CaL}}$  peak was upregulated mainly by PKA during ISO stimulation (by comparing physiological and BAPTA<sub>i</sub> conditions), whereas  $I_{\text{NaL}}$  was upregulated by PKA and CaMKII in an almost equal manner both in control and HF (Figure 6). Importantly, the ISO-induced increases in  $I_{\text{CaL}}$  and  $I_{\text{NaL}}$  were limited in HF both in physiological and BAPTA<sub>i</sub> conditions (Figure 6). While the ISO EC<sub>50</sub> for  $I_{\text{NaL}}$  activation was slightly increased in HF, the eventual maximal  $I_{\text{NaL}}$  density was the same in HF versus age-matched control, in part because of the increased basal  $I_{\text{NaL}}$  in HF (Figure 7A). On the other hand, the ISO EC<sub>50</sub> for  $I_{\text{CaL}}$  activation was not altered in HF, but the maximal effect was  $\approx 40\%$  smaller in HF versus age-matched control (Figure 7B) similar to prior report in this HF model.<sup>4</sup> This blunted  $\beta\text{AR}$  response could be due to reduced number of  $\beta_1\text{ARs}$ ,<sup>70</sup> lower local cAMP levels,<sup>71</sup> or altered phosphatases and phosphodiesterases in HF.<sup>52</sup>

$I_{\text{CaL}}$ ,  $I_{\text{NaL}}$ , and  $I_{\text{NCX}}$  reach their peak density sequentially during the AP, and their relative contributions to net inward current also dynamically change during the AP time course, as demonstrated previously in pig<sup>51</sup> and guinea-pig<sup>20, 31</sup> cardiomyocytes. In this study we demonstrated their detailed contribution in a chronic pressure/volume overload-induced HF rabbit model (Figure 8). The enhanced  $I_{\text{NaL}}$  and  $I_{\text{NCX}}$  increase the demand on the repolarizing  $\text{K}^+$  currents, that are also remodeled in HF.<sup>13, 14</sup> The balance between these depolarizing and repolarizing currents in HF is shifted during phase 3 of the AP so as to slow repolarization and prolong APD.<sup>51</sup>

## Conclusions

We measured  $I_{NaL}$  under physiologic recording conditions (AP-clamp with physiologic ionic composition, pacing rate,  $[Ca^{2+}]_i$  and temperature) and demonstrated a key role  $I_{NaL}$  enhancement in HF in APD prolongation and increased STV, especially at slow heart rates.  $I_{NaL}$  increase and its consequences may be exacerbated upon sympathetic activation. Our results agree with previous studies showing beneficial effects of  $I_{NaL}$  inhibition in HF and point to  $I_{NaL}$  as a therapeutic target to reduce the risk of arrhythmias in HF.<sup>18, 24</sup> However, it should be considered that selective  $I_{NaL}$  inhibition decreased APD, albeit more modestly, in control. On the other hand, hyporesponsiveness of  $I_{CaL}$  to  $\beta$ AR stimulation limits  $Ca^{2+}$  entry and that can aggravate the contractile deficit in HF. Our data demonstrate the importance of utilizing physiological recording conditions when measuring ionic currents, especially in cardiac pathologies associated with altered  $[Ca^{2+}]_i$  handling and CaMKII activity, in order to improve our understanding of electrophysiological remodeling and mechanistic bases of arrhythmogenesis in HF.

## Supplementary Material

Refer to Web version on PubMed Central for supplementary material.

## Acknowledgments:

We thank Dr William T. Ferrier and Linda Talken for performing the surgical procedures, and Lynette M. Mendoza for performing echocardiography. We also thank Logan R.J. Bailey, Johanna M. Borst, Austen J. Lucena, Maura Ferrero, Matthew L. Stein, Ian P. Palmer, and Maximilien Bergman for their help in animal care and cell isolation.

**Sources of Funding:** This work was supported by grants from the National Institute of Health P01-HL080101 and R01-HL030077 (Dr Bers), R01-HL142282 (Drs Bers and Bossuyt), OT2-OD023848, OT2-OD026580 and R01-HL131517, R01-HL141214 (Dr Grandi), R01-HL090880 (Drs Izu and Chen-Izu), R01-HL123526 (Dr Chen-Izu), and K99-HL138160 (Dr Morotti); the American Heart Association 14GRNT20510041 (Dr Chen-Izu), and 15SDG24910015 (Dr Grandi); the Hungarian Scientific Research Fund OTKA101196 (Dr Bányász); the Heart Rhythm Society post-doctoral fellowship 16OA9HRS (Dr Morotti); and the UC Davis School of Medicine Dean's Fellow award (Dr Grandi).

## References:

### References

1. Volders PG, Vos MA, Szabo B, Sipido KR, de Groot SH, Gorgels AP, Wellens HJ, Lazzara R. Progress in the understanding of cardiac early afterdepolarizations and torsades de pointes: Time to revise current concepts. *Cardiovasc Res.* 2000;46:376–392. [PubMed: 10912449]
2. Weiss JN, Garfinkel A, Karagueuzian HS, Chen PS, Qu Z. Early afterdepolarizations and cardiac arrhythmias. *Heart Rhythm.* 2010;7:1891–1899. [PubMed: 20868774]
3. Verkerk AO, Veldkamp MW, Baartscheer A, Schumacher CA, Klopping C, van Ginneken AC, Ravensloot JH. Ionic mechanism of delayed afterdepolarizations in ventricular cells isolated from human end-stage failing hearts. *Circulation.* 2001;104:2728–2733. [PubMed: 11723027]
4. Pogwizd SM, Schlotthauer K, Li L, Yuan W, Bers DM. Arrhythmogenesis and contractile dysfunction in heart failure: Roles of sodium-calcium exchange, inward rectifier potassium current, and residual beta-adrenergic responsiveness. *Circ Res.* 2001;88:1159–1167. [PubMed: 11397782]
5. Kaab S, Nuss HB, Chiamvimonvat N, O'Rourke B, Pak PH, Kass DA, Marban E, Tomaselli GF. Ionic mechanism of action potential prolongation in ventricular myocytes from dogs with pacing-induced heart failure. *Circ Res.* 1996;78:262–273. [PubMed: 8575070]

6. Tomaselli GF, Beuckelmann DJ, Calkins HG, Berger RD, Kessler PD, Lawrence JH, Kass D, Feldman AM, Marban E. Sudden cardiac death in heart failure. The role of abnormal repolarization. *Circulation*. 1994;90:2534–2539. [PubMed: 7955213]
7. Maltsev VA, Silverman N, Sabbah HN, Undrovinas AI. Chronic heart failure slows late sodium current in human and canine ventricular myocytes: Implications for repolarization variability. *Eur J Heart Fail*. 2007;9:219–227. [PubMed: 17067855]
8. Piccirillo G, Magri D, Matera S, Magnanti M, Torrini A, Pasquazzi E, Schifano E, Velitti S, Marigliano V, Quaglione R, Barilla F. Qt variability strongly predicts sudden cardiac death in asymptomatic subjects with mild or moderate left ventricular systolic dysfunction: A prospective study. *Eur Heart J*. 2007;28:1344–1350. [PubMed: 17101636]
9. Pogwizd SM, Qi M, Yuan WL, Samarel AM, Bers DM. Upregulation of Na<sup>+</sup>/Ca<sup>2+</sup> exchanger expression and function in an arrhythmogenic rabbit model of heart failure. *Circ. Res*. 1999;85:1009–1019. [PubMed: 10571531]
10. Weber CR, Piacentino V 3rd, Houser SR, Bers DM. Dynamic regulation of sodium/calcium exchange function in human heart failure. *Circulation*. 2003;108:2224–2229. [PubMed: 14557358]
11. Maltsev VA, Sabbah HN, Higgins RS, Silverman N, Lesch M, Undrovinas AI. Novel, ultraslow inactivating sodium current in human ventricular cardiomyocytes. *Circulation*. 1998;98:2545–2552. [PubMed: 9843461]
12. Valdivia CR, Chu WW, Pu J, Foell JD, Haworth RA, Wolff MR, Kamp TJ, Makielski JC. Increased late sodium current in myocytes from a canine heart failure model and from failing human heart. *J Mol Cell Cardiol*. 2005;38:475–483. [PubMed: 15733907]
13. Beuckelmann DJ, Nabauer M, Erdmann E. Alterations of K<sup>+</sup> currents in isolated human ventricular myocytes from patients with terminal heart failure. *Circ Res*. 1993;73:379–385. [PubMed: 8330380]
14. Hegyí B, Bossuyt J, Ginsburg KS, Mendoza LM, Talken L, Ferrier WT, Pogwizd SM, Izu LT, Chen-Izu Y, Bers DM. Altered repolarization reserve in failing rabbit ventricular myocytes: Calcium and beta-adrenergic effects on delayed- and inward-rectifier potassium currents. *Circ Arrhythm Electrophysiol*. 2018;11:e005852. [PubMed: 29437761]
15. Kaab S, Dixon J, Duc J, Ashen D, Nabauer M, Beuckelmann DJ, Steinbeck G, McKinnon D, Tomaselli GF. Molecular basis of transient outward potassium current downregulation in human heart failure - a decrease in Kv4.3 mRNA correlates with a reduction in current density. *Circulation*. 1998;98:1383–1393. [PubMed: 9760292]
16. Rivaud MR, Agullo-Pascual E, Lin X, Leo-Macias A, Zhang M, Rothenberg E, Bezzina CR, Delmar M, Remme CA. Sodium channel remodeling in subcellular microdomains of murine failing cardiomyocytes. *J Am Heart Assoc*. 2017;6.
17. Wagner S, Dybkova N, Rasenack EC, Jacobshagen C, Fabritz L, Kirchhof P, Maier SK, Zhang T, Hasenfuss G, Brown JH, Bers DM, Maier LS. Ca<sup>2+</sup>/calmodulin-dependent protein kinase II regulates cardiac Na<sup>+</sup> channels. *J Clin Invest*. 2006;116:3127–3138. [PubMed: 17124532]
18. Toischer K, Hartmann N, Wagner S, Fischer TH, Herting J, Danner BC, Sag CM, Hund TJ, Mohler PJ, Belardinelli L, Hasenfuss G, Maier LS, Sossalla S. Role of late sodium current as a potential arrhythmogenic mechanism in the progression of pressure-induced heart disease. *J Mol Cell Cardiol*. 2013;61:111–122. [PubMed: 23570977]
19. Koval OM, Snyder JS, Wolf RM, Pavlovicz RE, Glynn P, Curran J, Leymaster ND, Dun W, Wright PJ, Cardona N, Qian L, Mitchell CC, Boyden PA, Binkley PF, Li C, Anderson ME, Mohler PJ, Hund TJ. Ca<sup>2+</sup>/calmodulin-dependent protein kinase II-based regulation of voltage-gated Na<sup>+</sup> channel in cardiac disease. *Circulation*. 2012;126:2084–2094. [PubMed: 23008441]
20. Horvath B, Banyasz T, Jian Z, Hegyí B, Kistamas K, Nanasi PP, Izu LT, Chen-Izu Y. Dynamics of the late Na<sup>(+)</sup> current during cardiac action potential and its contribution to afterdepolarizations. *J Mol Cell Cardiol*. 2013;64:59–68. [PubMed: 24012538]
21. Hegyí B, Banyasz T, Izu LT, Belardinelli L, Bers DM, Chen-Izu Y. Beta-adrenergic regulation of late Na<sup>(+)</sup> current during cardiac action potential is mediated by both PKA and CaMKII. *J Mol Cell Cardiol*. 2018;123:168–179. [PubMed: 30240676]
22. Matsuda JJ, Lee H, Shibata EF. Enhancement of rabbit cardiac sodium channels by beta-adrenergic stimulation. *Circ Res*. 1992;70:199–207. [PubMed: 1309315]

23. Belardinelli L, Giles WR, Rajamani S, Karagueuzian HS, Shryock JC. Cardiac late Na(+) current: Proarrhythmic effects, roles in long QT syndromes, and pathological relationship to CaMKII and oxidative stress. *Heart Rhythm*. 2015;12:440–448. [PubMed: 25460862]
24. Sag CM, Mallwitz A, Wagner S, Hartmann N, Schotola H, Fischer TH, Ungeheuer N, Herting J, Shah AM, Maier LS, Sossalla S, Unsold B. Enhanced late *I*<sub>Na</sub> induces proarrhythmic SR Ca leak in a CaMKII-dependent manner. *J Mol Cell Cardiol*. 2014;76:94–105. [PubMed: 25173923]
25. Tomaselli GF, Marban E. Electrophysiological remodeling in hypertrophy and heart failure. *Cardiovasc Res*. 1999;42:270–283. [PubMed: 10533566]
26. Nattel S, Maguy A, Le Bouter S, Yeh YH. Arrhythmogenic ion-channel remodeling in the heart: Heart failure, myocardial infarction, and atrial fibrillation. *Physiol Rev*. 2007;87:425–456. [PubMed: 17429037]
27. Anderson ME, Braun AP, Schulman H, Premack BA. Multifunctional Ca<sup>2+</sup>/calmodulin-dependent protein-kinase mediates Ca<sup>2+</sup>-induced enhancement of the L-type Ca<sup>2+</sup> current in rabbit ventricular myocytes. *Circ Res*. 1994;75:854–861. [PubMed: 7923631]
28. Hudmon A, Schulman H, Kim J, Maltez JM, Tsien RW, Pitt GS. CaMKII tethers to L-type Ca<sup>2+</sup> channels, establishing a local and dedicated integrator of Ca<sup>2+</sup> signals for facilitation. *J Cell Biol*. 2005;171:537–547. [PubMed: 16275756]
29. Bers DM, Morotti S. Ca(2+) current facilitation is CaMKII-dependent and has arrhythmogenic consequences. *Front Pharmacol*. 2014;5:144. [PubMed: 24987371]
30. Hoeker GS, Hanafy MA, Oster RA, Bers DM, Pogwizd SM. Reduced arrhythmia inducibility with calcium/calmodulin-dependent protein kinase II inhibition in heart failure rabbits. *J Cardiovasc Pharmacol*. 2016;67:260–265. [PubMed: 26650851]
31. Banyasz T, Horvath B, Jian Z, Izu LT, Chen-Izu Y. Profile of L-type Ca(2+) current and Na(+)/Ca(2+) exchange current during cardiac action potential in ventricular myocytes. *Heart Rhythm*. 2012;9:134–142. [PubMed: 21884673]
32. Horvath B, Vaczi K, Hegyi B, Gonczi M, Dienes B, Kistamas K, Banyasz T, Magyar J, Baczko I, Varro A, Seprenyi G, Csernoch L, Nanasi PP, Szentandrassy N. Sarcolemmal Ca(2+)-entry through L-type Ca(2+) channels controls the profile of Ca(2+)-activated Cl(-) current in canine ventricular myocytes. *J Mol Cell Cardiol*. 2016;97:125–139. [PubMed: 27189885]
33. Szentandrassy N, Kistamas K, Hegyi B, Horvath B, Ruzsnavszky F, Vaczi K, Magyar J, Banyasz T, Varro A, Nanasi PP. Contribution of ion currents to beat-to-beat variability of action potential duration in canine ventricular myocytes. *Pflugers Arch*. 2015;467:1431–1443. [PubMed: 25081243]
34. Chen-Izu Y, Izu LT, Hegyi B, Bányász T. Recording of ionic currents under physiological conditions: Action potential-clamp and ‘onion-peeling’ techniques In: Jue T, ed. *Modern Tools of Biophysics*. New York, NY: Springer New York; 2017:31–48.
35. Banyasz T, Horvath B, Jian Z, Izu LT, Chen-Izu Y. Sequential dissection of multiple ionic currents in single cardiac myocytes under action potential-clamp. *J Mol Cell Cardiol*. 2011;50:578–581. [PubMed: 21215755]
36. Bartos DC, Morotti S, Ginsburg KS, Grandi E, Bers DM. Quantitative analysis of the Ca<sup>2+</sup>-dependent regulation of delayed rectifier K<sup>+</sup> current I<sub>Ks</sub> in rabbit ventricular myocytes. *J Physiol*. 2017;595:2253–2268. [PubMed: 28008618]
37. Shannon TR, Wang F, Puglisi J, Weber C, Bers DM. A mathematical treatment of integrated Ca dynamics within the ventricular myocyte. *Biophys J*. 2004;87:3351–3371. [PubMed: 15347581]
38. Soltis AR, Saucerman JJ. Synergy between CaMKII substrates and beta-adrenergic signaling in regulation of cardiac myocyte Ca(2+) handling. *Biophys J*. 2010;99:2038–2047. [PubMed: 20923637]
39. Negroni JA, Morotti S, Lascano EC, Gomes AV, Grandi E, Puglisi JL, Bers DM. Beta-adrenergic effects on cardiac myofilaments and contraction in an integrated rabbit ventricular myocyte model. *J Mol Cell Cardiol*. 2015;81:162–175. [PubMed: 25724724]
40. Shannon TR, Wang F, Bers DM. Regulation of cardiac sarcoplasmic reticulum Ca release by luminal [Ca] and altered gating assessed with a mathematical model. *Biophys J*. 2005;89:4096–4110. [PubMed: 16169970]

41. Despa S, Islam MA, Weber CR, Pogwizd SM, Bers DM. Intracellular Na<sup>+</sup> concentration is elevated in heart failure but Na/K pump function is unchanged. *Circulation*. 2002;105:2543–2548. [PubMed: 12034663]
42. Huang B, El-Sherif T, Gidh-Jain M, Qin D, El-Sherif N. Alterations of sodium channel kinetics and gene expression in the postinfarction remodeled myocardium. *J Cardiovasc Electrophysiol*. 2001;12:218–225. [PubMed: 11232622]
43. Mishra S, Reznikov V, Maltsev VA, Undrovinas NA, Sabbah HN, Undrovinas A. Contribution of sodium channel neuronal isoform Na(v)1.1 to late sodium current in ventricular myocytes from failing hearts. *J Physiol*. 2015;593:1409–1427. [PubMed: 25772296]
44. Clancy CE, Chen-Izu Y, Bers DM, Belardinelli L, Boyden PA, Csernoch L, Despa S, Fermini B, Hool LC, Izu L, Kass RS, Lederer WJ, Louch WE, Maack C, Matiazzi A, Qu Z, Rajamani S, Ripinger CM, Sejersted OM, O'Rourke B, Weiss JN, Varro A, Zaza A. Deranged sodium to sudden death. *J Physiol*. 2015;593:1331–1345. [PubMed: 25772289]
45. Wagner S, Ruff HM, Weber SL, Bellmann S, Sowa T, Schulte T, Anderson ME, Grandi E, Bers DM, Backs J, Belardinelli L, Maier LS. Reactive oxygen species-activated Ca/calmodulin kinase II $\delta$  is required for late I(Na) augmentation leading to cellular Na and Ca overload. *Circ Res*. 2011;108:555–565. [PubMed: 21252154]
46. Morotti S, Edwards AG, McCulloch AD, Bers DM, Grandi E. A novel computational model of mouse myocyte electrophysiology to assess the synergy between Na<sup>+</sup> loading and CaMKII. *J Physiol*. 2014;592:1181–1197. [PubMed: 24421356]
47. Schroder F, Handrock R, Beuckelmann DJ, Hirt S, Hullin R, Priebe L, Schwinger RH, Weil J, Herzig S. Increased availability and open probability of single L-type calcium channels from failing compared with nonfailing human ventricle. *Circulation*. 1998;98:969–976. [PubMed: 9737516]
48. Findlay I Voltage- and cation-dependent inactivation of L-type Ca<sup>2+</sup> channel currents in guinea-pig ventricular myocytes. *J Physiol*. 2002;541:731–740. [PubMed: 12068036]
49. Weber CR, Piacentino V, Ginsburg KS, Houser SR, Bers DM. Na<sup>+</sup>-Ca<sup>2+</sup> exchange current and submembrane [Ca<sup>2+</sup>] during the cardiac action potential. *Circ Res*. 2002;90:182–189. [PubMed: 11834711]
50. Grandi E, Pasqualini FS, Bers DM. A novel computational model of the human ventricular action potential and ca transient. *J Mol Cell Cardiol*. 2010;48:112–121. [PubMed: 19835882]
51. Hegyi B, Bossuyt J, Griffiths LG, Shimkunas R, Coulibaly Z, Jian Z, Grimsrud KN, Sondergaard CS, Ginsburg KS, Chiamvimonvat N, Belardinelli L, Varro A, Papp JG, Pollesello P, Levijoki J, Izu LT, Boyd WD, Banyasz T, Bers DM, Chen-Izu Y. Complex electrophysiological remodeling in postinfarction ischemic heart failure. *Proc Natl Acad Sci U S A*. 2018;115:E3036–E3044. [PubMed: 29531045]
52. Ai X, Curran JW, Shannon TR, Bers DM, Pogwizd SM. Ca<sup>2+</sup>/calmodulin-dependent protein kinase modulates cardiac ryanodine receptor phosphorylation and sarcoplasmic reticulum Ca<sup>2+</sup> leak in heart failure. *Circ Res*. 2005;97:1314–1322. [PubMed: 16269653]
53. Curran J, Brown KH, Santiago DJ, Pogwizd S, Bers DM, Shannon TR. Spontaneous Ca waves in ventricular myocytes from failing hearts depend on Ca(2+)-calmodulin-dependent protein kinase II. *J Mol Cell Cardiol*. 2010;49:25–32. [PubMed: 20353795]
54. Vermeulen JT, McGuire MA, Ophof T, Coronel R, de Bakker JM, Klopping C, Janse MJ. Triggered activity and automaticity in ventricular trabeculae of failing human and rabbit hearts. *Cardiovasc Res*. 1994;28:1547–1554. [PubMed: 8001044]
55. Davey PP, Barlow C, Hart G. Prolongation of the QT interval in heart failure occurs at low but not at high heart rates. *Clin Sci (Lond)*. 2000;98:603–610. [PubMed: 10781393]
56. Wu L, Ma J, Li H, Wang C, Grandi E, Zhang P, Luo A, Bers DM, Shryock JC, Belardinelli L. Late sodium current contributes to the reverse rate-dependent effect of IKr inhibition on ventricular repolarization. *Circulation*. 2011;123:1713–1720. [PubMed: 21482963]
57. Baartscheer A, Schumacher CA, Belterman CN, Coronel R, Fiolet JW. SR calcium handling and calcium after-transients in a rabbit model of heart failure. *Cardiovasc Res*. 2003;58:99–108. [PubMed: 12667950]

58. Johnson DM, Heijman J, Bode EF, Greensmith DJ, van der Linde H, Abi-Gerges N, Eisner DA, Trafford AW, Volders PG. Diastolic spontaneous calcium release from the sarcoplasmic reticulum increases beat-to-beat variability of repolarization in canine ventricular myocytes after beta-adrenergic stimulation. *Circ Res.* 2013;112:246–256. [PubMed: 23149594]
59. Gomez JF, Cardona K, Trenor B. Lessons learned from multi-scale modeling of the failing heart. *J Mol Cell Cardiol.* 2015;89:146–159. [PubMed: 26476237]
60. Hegyí B, Bers DM, Bossuyt J. CaMKII signaling in heart diseases: Emerging role in diabetic cardiomyopathy. *J Mol Cell Cardiol.* 2019;127:246–259. [PubMed: 30633874]
61. Peterson BZ, DeMaria CD, Adelman JP, Yue DT. Calmodulin is the Ca<sup>2+</sup> sensor for Ca<sup>2+</sup>-dependent inactivation of L-type calcium channels. *Neuron.* 1999;22:549–558. [PubMed: 10197534]
62. Grandi E, Morotti S, Ginsburg KS, Severi S, Bers DM. Interplay of voltage and Ca-dependent inactivation of L-type Ca current. *Prog Biophys Mol Biol.* 2010;103:44–50. [PubMed: 20184915]
63. Sarhan MF, Tung CC, Van Petegem F, Ahern CA. Crystallographic basis for calcium regulation of sodium channels. *Proc Natl Acad Sci U S A.* 2012;109:3558–3563. [PubMed: 22331908]
64. Maltsev VA, Reznikov V, Undrovinas NA, Sabbah HN, Undrovinas A. Modulation of late sodium current by Ca<sup>2+</sup>, calmodulin, and CaMKII in normal and failing dog cardiomyocytes: Similarities and differences. *Am J Physiol Heart Circ Physiol.* 2008;294:H1597–1608. [PubMed: 18203851]
65. Chen-Izu Y, Shaw RM, Pitt GS, Yarov-Yarovoy V, Sack JT, Abriel H, Aldrich RW, Belardinelli L, Cannell MB, Catterall WA, Chazin WJ, Chiamvimonvat N, Deschenes I, Grandi E, Hund TJ, Izu LT, Maier LS, Maltsev VA, Marionneau C, Mohler PJ, Rajamani S, Rasmusson RL, Sobie EA, Clancy CE, Bers DM. Na<sup>+</sup> channel function, regulation, structure, trafficking and sequestration. *J Physiol.* 2015;593:1347–1360. [PubMed: 25772290]
66. Hullin R, Matthes J, von Vietinghoff S, Bodi I, Rubio M, D'Souza K, Friedrich Khan I, Rottlander D, Hoppe UC, Mohacsi P, Schmitteckert E, Gilsbach R, Bunemann M, Hein L, Schwartz A, Herzog S. Increased expression of the auxiliary beta(2)-subunit of ventricular L-type Ca(2)<sup>+</sup> channels leads to single-channel activity characteristic of heart failure. *PLoS One.* 2007;2:e292. [PubMed: 17356701]
67. Colecraft HM, Alseikhan B, Takahashi SX, Chaudhuri D, Mittman S, Yegnasubramanian V, Alvania RS, Johns DC, Marban E, Yue DT. Novel functional properties of Ca(2<sup>+</sup>) channel beta subunits revealed by their expression in adult rat heart cells. *J Physiol.* 2002;541:435–452. [PubMed: 12042350]
68. Miriyala J, Nguyen T, Yue DT, Colecraft HM. Role of CaVbeta subunits, and lack of functional reserve, in protein kinase A modulation of cardiac CaV1.2 channels. *Circ Res.* 2008;102:e54–64. [PubMed: 18356540]
69. Beetz N, Hein L, Meszaros J, Gilsbach R, Barreto F, Meissner M, Hoppe UC, Schwartz A, Herzog S, Matthes J. Transgenic simulation of human heart failure-like L-type Ca<sup>2+</sup>-channels: Implications for fibrosis and heart rate in mice. *Cardiovasc Res.* 2009;84:396–406. [PubMed: 19620129]
70. Desantiago J, Ai X, Islam M, Acuna G, Ziolo MT, Bers DM, Pogwizd SM. Arrhythmogenic effects of beta<sub>2</sub>-adrenergic stimulation in the failing heart are attributable to enhanced sarcoplasmic reticulum Ca load. *Circ Res.* 2008;102:1389–1397. [PubMed: 18467626]
71. Barbagallo F, Xu B, Reddy GR, West T, Wang Q, Fu Q, Li M, Shi Q, Ginsburg KS, Ferrier W, Isidori AM, Naro F, Patel HH, Bossuyt J, Bers D, Xiang YK. Genetically encoded biosensors reveal pka hyperphosphorylation on the myofilaments in rabbit heart failure. *Circ Res.* 2016;119:931–943. [PubMed: 27576469]
72. Katchman A, Yang L, Zakharov SI, Kushner J, Abrams J, Chen BX, Liu G, Pitt GS, Colecraft HM, Marx SO. Proteolytic cleavage and PKA phosphorylation of alpha1C subunit are not required for adrenergic regulation of CaV1.2 in the heart. *Proc Natl Acad Sci U S A.* 2017;114:9194–9199. [PubMed: 28784807]
73. Herren AW, Weber DM, Rigor RR, Margulies KB, Phinney BS, Bers DM. CaMKII phosphorylation of Na(V)1.5: Novel in vitro sites identified by mass spectrometry and reduced S516 phosphorylation in human heart failure. *J Proteome Res.* 2015;14:2298–2311. [PubMed: 25815641]

**What is Known:**

- Significant ion channel remodeling occurs in heart failure (HF) which results in prolongation of the cardiac action potential (and QT interval in ECG) and increases the risk of arrhythmias.
- Enhanced late Na<sup>+</sup> current and upregulation of Na<sup>+</sup>/Ca<sup>2+</sup> exchanger (NCX) have been reported in HF.

**What the Study Adds:**

- CaMKII-dependent and beta-adrenergic upregulation of late Na<sup>+</sup> current in HF enhances the net depolarization drive and significantly contributes to arrhythmogenic action potential alterations in HF.
- Reveal CaMKII-dependent facilitation but β-adrenergic hypo-responsiveness of L-type Ca<sup>2+</sup> current in HF.

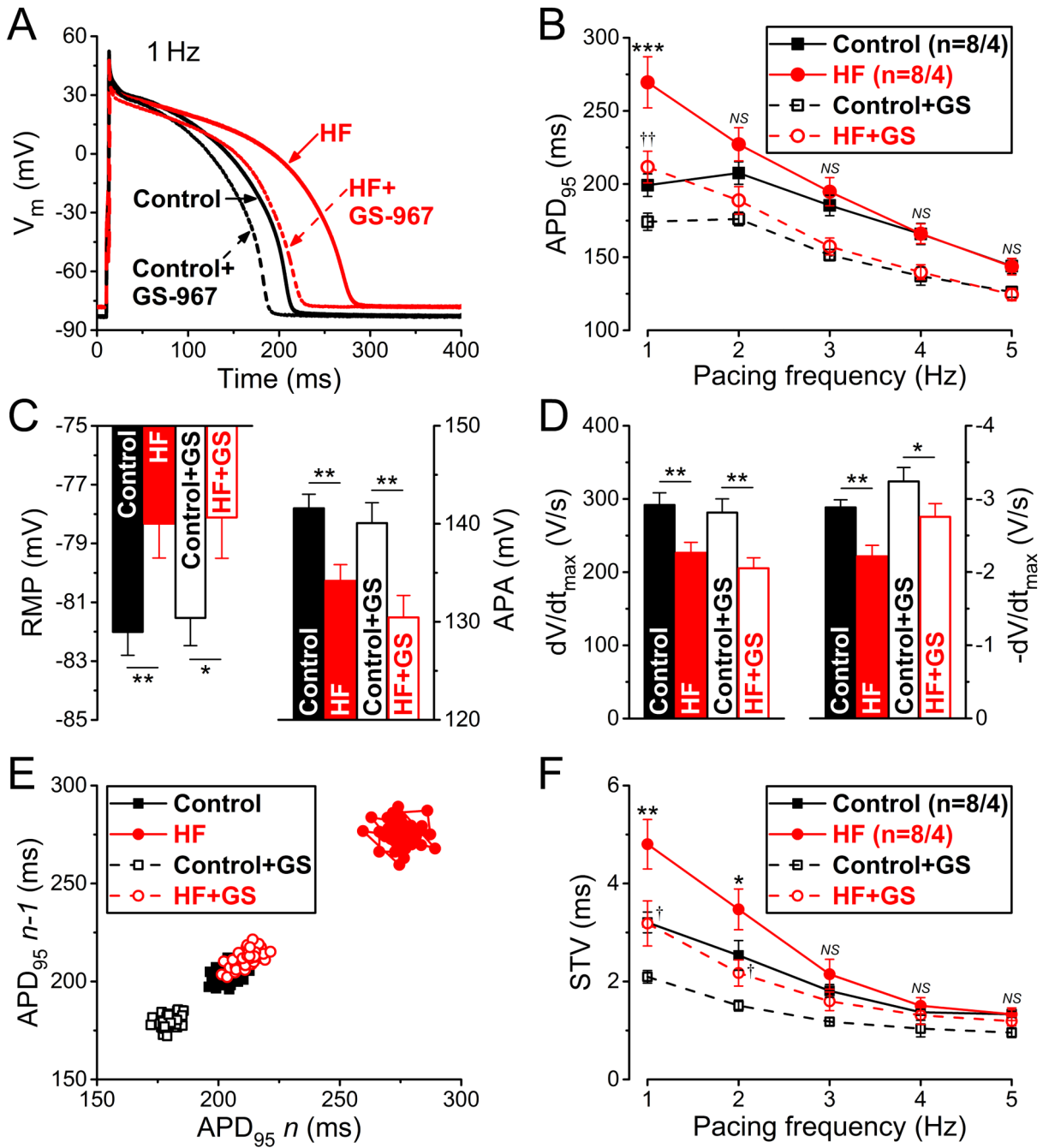


**Figure 1.**

Frequency-dependent effects of late Na<sup>+</sup> current inhibition on action potential (AP) in heart failure (HF). **A** Representative APs recorded at 1 Hz steady-state pacing in HF and age-matched control before and after treatment with the selective late Na<sup>+</sup> current inhibitor GS-967 (1 μmol/L). **B** Frequency-dependence of AP duration measured at 95% of repolarization (APD<sub>95</sub>). **C** Resting membrane potential (RMP) was slightly more positive in HF in line with decreased AP amplitude (APA) at 1 Hz pacing. GS-967 (GS) had no effect on either AP parameters. **D** Maximal rate of rise (dV/dt<sub>max</sub>) and maximal rate of phase 3

repolarization ( $-dV/dt_{\max}$ ) were significantly decreased in HF compared to control. GS increased  $-dV/dt_{\max}$  already in control but even more in HF. **E** Representative Poincaré plots of 50 consecutive  $APD_{95}$  values at 1 Hz pacing. **F** Frequency-dependent short-term variability of  $APD_{95}$  (STV). STV was increased at low pacing frequencies in HF, which was decreased with GS to the control level. Columns and bars represent mean $\pm$ SEM. *n* refers to cells/animals measured in each group. Paired and unpaired Student's *t* tests following analysis of variance (ANOVA). \**P*<0.05, \*\**P*<0.01, \*\*\**P*<0.001 versus control; †*P*<0.05, ††*P*<0.01 versus control+GS-967.

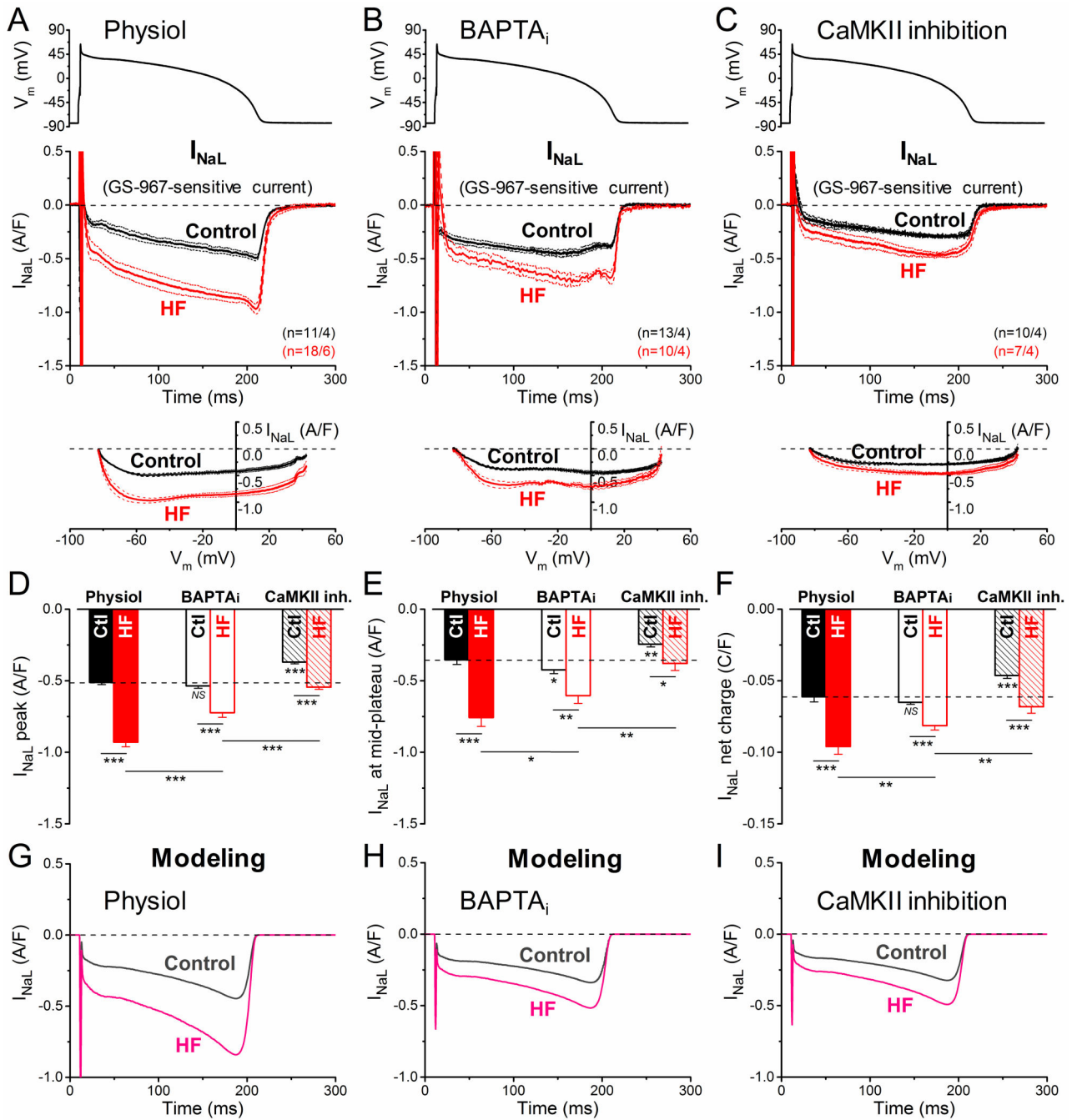


**Figure 2.**

Ca<sup>2+</sup>/calmodulin-dependent protein kinase II (CaMKII)-dependent upregulation of late Na<sup>+</sup> current (I<sub>NaL</sub>) in heart failure (HF) under action potential (AP)-clamp. I<sub>NaL</sub> was measured as GS-967 (1 μM)-sensitive current in HF and age-matched control. AP-clamp using a prerecorded typical AP (shown above) was applied at 2 Hz pacing. **A** I<sub>NaL</sub> traces (mean ± SEM) recorded under preserved [Ca<sup>2+</sup>]<sub>i</sub> cycling (physiol). I<sub>NaL</sub> was significantly increased already during the early plateau phase of the AP and it achieved a nearly doubled peak density during phase 3 repolarization in HF cells having Ca<sup>2+</sup> transients. Current-voltage

relationship under AP-clamp is shown below. **B**  $I_{NaL}$  traces (mean±SEM) recorded under buffered  $[Ca^{2+}]_i$  using 10 mmol/L BAPTA in the pipette (BAPTA<sub>i</sub>). Buffering  $[Ca^{2+}]_i$  significantly reduced  $I_{NaL}$  peak density in HF. **C**  $I_{NaL}$  traces (mean±SEM) recorded in cells pretreated with the specific CaMKII inhibitor AIP (autocamtide-2-related inhibitory peptide; 1 μmol/L). AIP reduced  $I_{NaL}$  in HF to the untreated control level; however, AIP also decreased  $I_{NaL}$  in control. **D** Peak  $I_{NaL}$  density was significantly upregulated in HF under AP, partially by a CaMKII-dependent acute effect on  $I_{NaL}$ . **E**  $I_{NaL}$  density measured at the mid-plateau of the AP. **F** Net charges carried by  $I_{NaL}$  under AP in HF and age-matched control. Columns and bars represent mean±SEM. *n* refers to cells/animals measured in each group. Analysis of variance (ANOVA) with Bonferroni posttest, \**P*<0.05, \*\**P*<0.01, \*\*\**P*<0.001. Ctl indicates control. **G-I** Simulated time courses of  $I_{NaL}$  under AP-clamp in control and HF obtained with physiol, BAPTA<sub>i</sub> and CaMKII inhibition conditions.

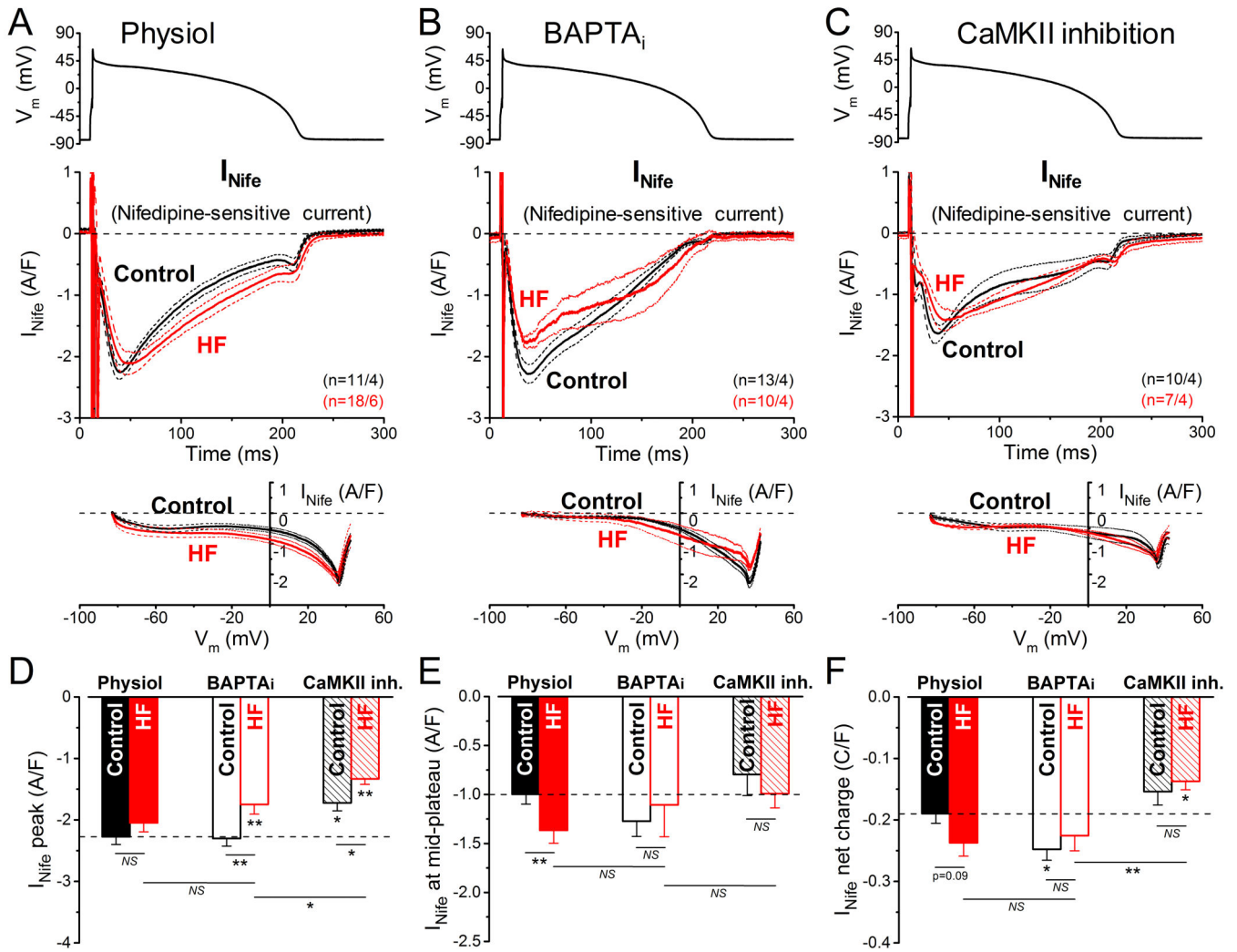


**Figure 3.** Nifedipine-sensitive current in heart failure (HF) under action potential (AP)-clamp. The L-type  $Ca^{2+}$  current and the inward  $Na^+/Ca^{2+}$  exchange current under action potential (AP) were measured as a composite nifedipine-sensitive current ( $I_{Nife}$ ) in HF and age-matched control. AP-clamp using a prerecorded typical AP (shown above) was applied at 2 Hz pacing before and after application of 10  $\mu$ mol/L nifedipine (Nife). **A**  $I_{Nife}$  traces (mean  $\pm$  SEM) recorded under preserved  $[Ca^{2+}]_i$  cycling (physiol).  $I_{Nife}$  was increased during the mid-plateau and the late-plateau phases of the AP in HF. Current-voltage relationship under AP-clamp is shown below.  $I_{Nife}$  traces (mean  $\pm$  SEM) recorded under buffered  $[Ca^{2+}]_i$  using 10 mmol/L BAPTA in the pipette (BAPTA<sub>i</sub>). Buffering  $[Ca^{2+}]_i$  significantly reduced  $I_{Nife}$  peak density in HF. **C**  $I_{Nife}$  traces (mean  $\pm$  SEM) recorded in cells pretreated with the specific CaMKII ( $Ca^{2+}$ /calmodulin-dependent protein kinase II) inhibitor AIP (autocamtide-2-related inhibitory peptide; 1  $\mu$ mol/L). AIP slightly reduced  $I_{Nife}$  peak density in HF. **D** Peak  $I_{Nife}$  density was significantly upregulated in HF under AP by CaMKII. **E**  $I_{Nife}$  density measured at the mid-plateau of the AP. **F** Net charges carried by  $I_{Nife}$  under AP in HF and age-matched control. Columns and bars represent mean  $\pm$  SEM. *n* refers to cells/animals

measured in each group. Analysis of variance (ANOVA) with Bonferroni posttest, \* $P < 0.05$ , \*\* $P < 0.01$ , \*\*\* $P < 0.001$ .

Author Manuscript

Author Manuscript

Author Manuscript

Author Manuscript

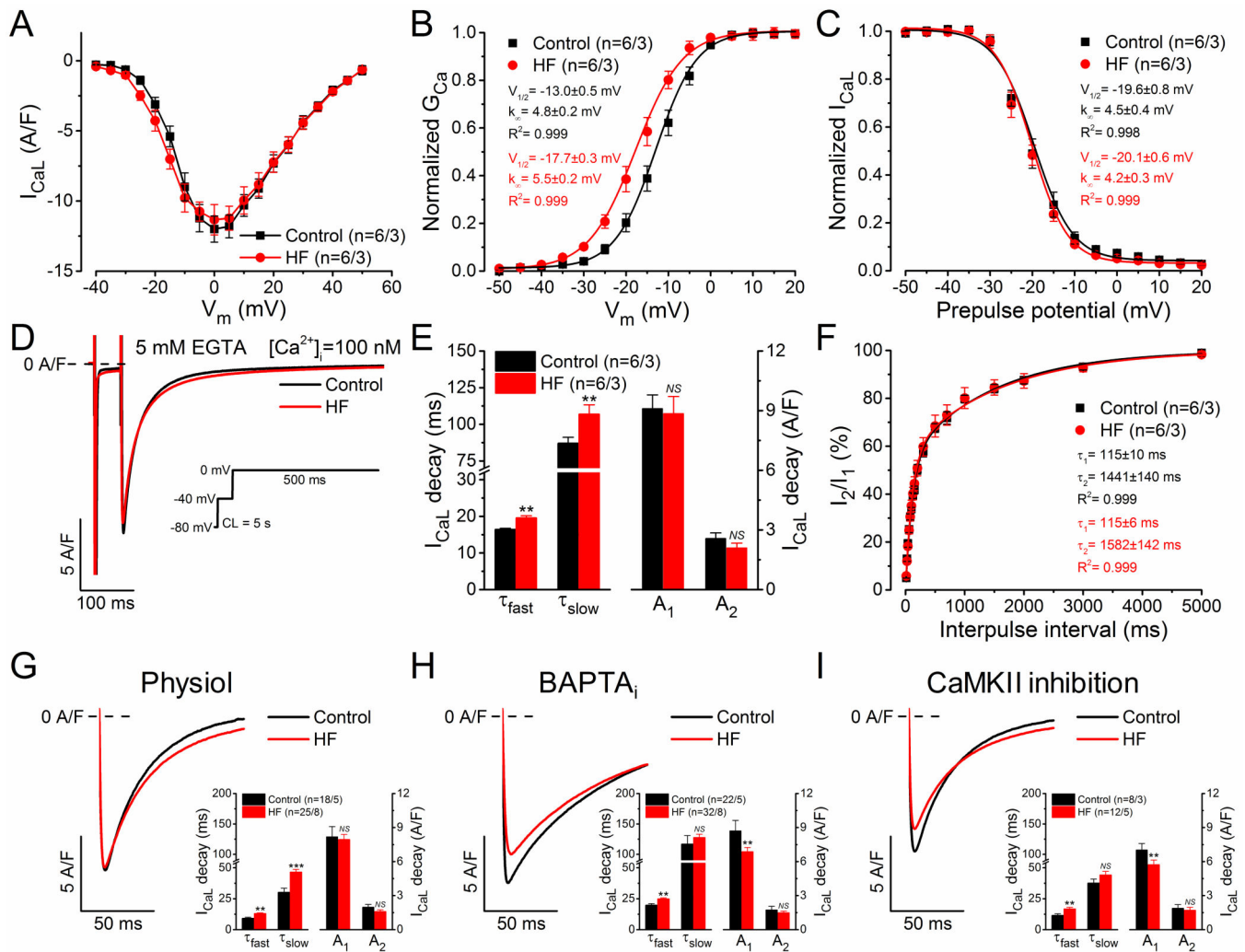


**Figure 4.**

Biophysical properties of L-type  $Ca^{2+}$  current ( $I_{CaL}$ ) in heart failure (HF). **A** Current-voltage relationship of  $I_{CaL}$  peak density in HF and age-matched control.  $I_{CaL}$  was measured in the presence of 5 mmol/L EGTA ( $[Ca^{2+}]_i=100$  nmol/L) in the pipette. **B** Steady-state activation of  $I_{CaL}$  was shifted by 5 mV to more negative potentials in HF. **C** Steady-state inactivation of  $I_{CaL}$  was unaltered in HF. **D** Representative  $I_{CaL}$  traces elicited by depolarization pulses to 0 mV (voltage protocol shown in the inset). **E** Decay time constants ( $\tau_{fast}$ ,  $\tau_{slow}$ ) of  $I_{CaL}$  were slightly increased in HF. **F**  $I_{CaL}$  recovery from inactivation was unchanged in HF. **G** Representative  $I_{CaL}$  traces under preserved  $[Ca^{2+}]_i$  cycling (physiol).  $I_{CaL}$  was elicited with depolarization pulse to 0 mV at 2 Hz. Inset shows significantly increased decay time constants but unaltered  $I_{CaL}$  amplitude in HF. **H** Representative  $I_{CaL}$  traces under buffered  $[Ca^{2+}]_i$  using 10 mmol/L BAPTA in the pipette (BAPTA<sub>i</sub>). Inset shows that the amplitude of the fast  $I_{CaL}$  decay was significantly reduced in HF versus control, whereas  $\tau_{fast}$  was still slightly increased in HF. **I** Representative  $I_{CaL}$  traces following specific CaMKII inhibition with AIP (1  $\mu$ mol/L). Inset shows the decay time constants of  $I_{CaL}$  and the corresponding amplitudes. The inactivation time course of  $I_{CaL}$  was fitted by a biexponential function.

Columns and bars represent mean±SEM. *n* refers to cells/animals measured in each group. Analysis of variance (ANOVA) with Bonferroni posttest, \**P*<0.05, \*\**P*<0.01, \*\*\**P*<0.001.

Author Manuscript

Author Manuscript

Author Manuscript

Author Manuscript

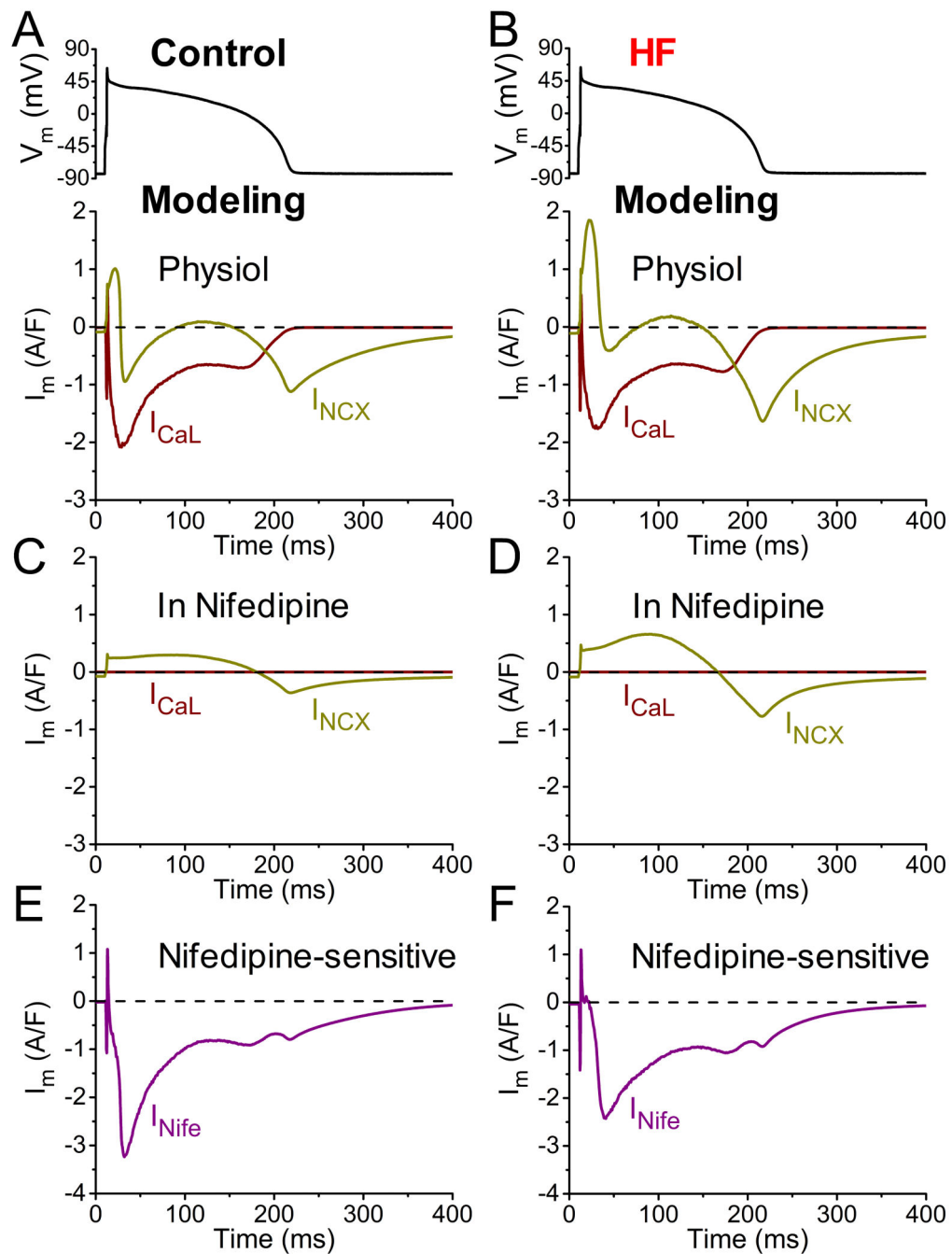


**Figure 5.** Simulated time courses of L-type  $Ca^{2+}$  current ( $I_{CaL}$ ) and  $Na^+/Ca^{2+}$  exchanger current ( $I_{NCX}$ ) under action potential (AP)-clamp in heart failure (HF). Simulated  $I_{CaL}$  and  $I_{NCX}$  have been obtained with our updated rabbit ventricular myocyte model that integrates detailed descriptions of electrophysiology,  $Ca^{2+}$  and  $Na^+$  handling, PKA and CaMKII signaling, and myofilament contraction. **A-B** Simulated  $I_{CaL}$  and  $I_{NCX}$  under AP-clamp at 2 Hz pacing in control (*left*) and HF (*right*) with physiological  $Ca^{2+}$  handling. **C-D** Simulated  $I_{CaL}$  and  $I_{NCX}$  after nifedipine (Nife) treatment (simulated assuming complete block of  $I_{CaL}$ )

under AP-clamp at 2 Hz pacing in control and HF. **E-F** Nifedipine-sensitive current ( $I_{\text{Nife}}$ ) expressed as sum of the changes in simulated  $I_{\text{CaL}}$  and  $I_{\text{NCX}}$  before and after nifedipine treatment in control and HF.

Author Manuscript

Author Manuscript

Author Manuscript

Author Manuscript

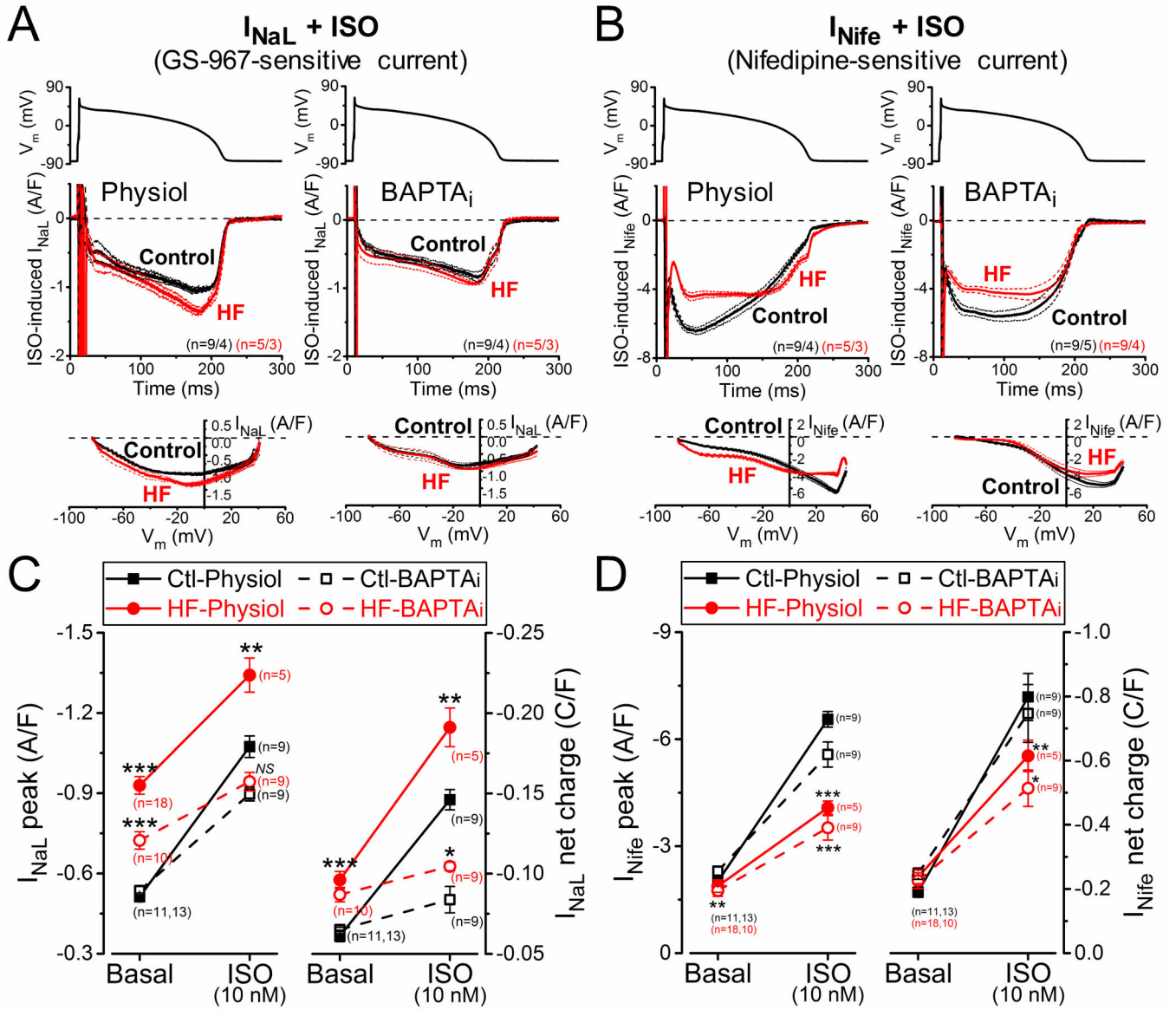


**Figure 6.** Altered response of inward currents to  $\beta$ -adrenergic receptor ( $\beta$ BAR) stimulation in heart failure (HF). The late  $Na^+$  current ( $I_{NaL}$ ) and the nifedipine-sensitive current ( $I_{Nife}$ ) were recorded after 2-min pretreatment with  $\beta$ BAR agonist isoproterenol (ISO, 10 nmol/L). **A**  $I_{NaL}$  traces (mean $\pm$ SEM) under AP-clamp at 2 Hz pacing measured with preserved  $[Ca^{2+}]_i$  cycling (physiol) and  $[Ca^{2+}]_i$  buffering using 10 mmol/L BAPTA in the pipette (BAPTA<sub>i</sub>) after ISO pretreatment in HF and age-matched control. Current-voltage relationship under AP-clamp is shown below. **B**  $I_{Nife}$  traces (mean $\pm$ SEM) under AP-clamp after ISO pretreatment in HF and age-matched control. **C** Upregulation of  $I_{NaL}$  peak and net charge induced by ISO, which was reduced with BAPTA<sub>i</sub>. **D** Robust increase in  $I_{Nife}$  after ISO stimulation, which was reduced in BAPTA<sub>i</sub>, indicating a  $Ca^{2+}$ -dependent pathway in mediating the response of  $\beta$ BAR stimulation on  $I_{Nife}$  (besides the classical protein kinase A effect). HF cells exhibited significantly reduced response of  $I_{Nife}$  after ISO stimulation both

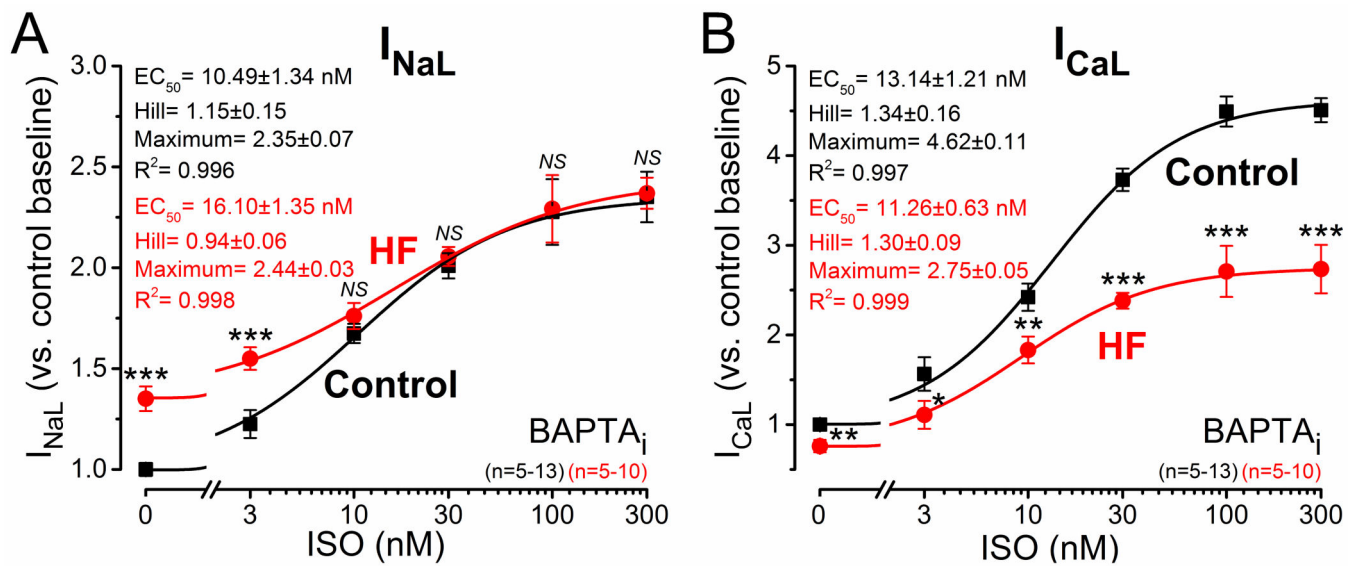
with and without  $[Ca^{2+}]_i$  buffering. Symbols and bars represent mean $\pm$ SEM.  $n$  refers to cells measured in each group, and the cells in each group came from 3 to 6 individual animals. Analysis of variance (ANOVA) with Bonferroni posttest, \* $P<0.05$ , \*\* $P<0.01$ , \*\*\* $P<0.001$ .

Author Manuscript

Author Manuscript

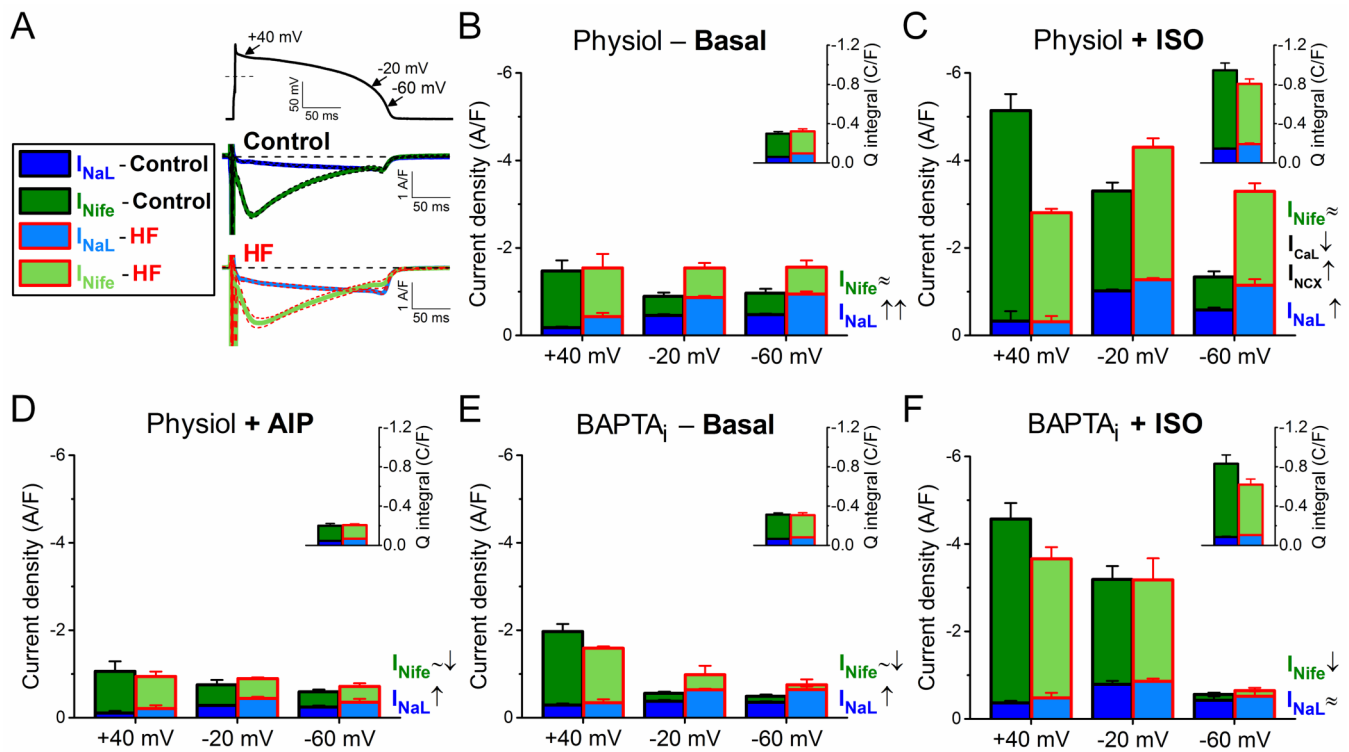
Author Manuscript

Author Manuscript



**Figure 7.**

$\beta$ -adrenergic receptor ( $\beta$ AR) responsiveness of inward currents in heart failure (HF). Dose-response effect of isoproterenol (ISO) on late  $Na^+$  current ( $I_{NaL}$ ) and L-type  $Ca^{2+}$  current ( $I_{CaL}$ ) peak densities under AP-clamp at 2 Hz pacing rate. Pipette solution contained 10 mmol/L BAPTA (BAPTA<sub>i</sub>). **A**  $I_{NaL}$  measured as GS-967-sensitive current significantly increased after ISO application.  $I_{NaL}$  sensitivity ( $EC_{50}$ , half maximal effective concentration) to ISO was slightly reduced in HF, and  $I_{NaL}$  exhibited similar maximal response in HF than in control despite the increased basal  $I_{NaL}$  in HF. **B**  $I_{CaL}$  measured as nifedipine-sensitive current was markedly increased after ISO treatment; however, the magnitude of the response was significantly blunted in HF with no change in ISO-sensitivity.  $EC_{50}$  values, Hill coefficients and maximum responses were determined by fitting data to the Hill equation, indicated by solid lines. Symbols and bars represent mean  $\pm$  SEM.  $n$  refers to the number of cells measured in each group, and the cells in each group came from 3 to 6 individual animals. Analysis of variance (ANOVA) with Bonferroni posttest, \* $P < 0.05$ , \*\* $P < 0.01$ , \*\*\* $P < 0.001$ .

**Figure 8.**

Relative contribution of inward currents to net depolarizing current in heart failure (HF).

Relative contributions and magnitudes of the major inward currents ( $I_{NaL}$  and  $I_{Nife}$ ) are compared in distinct phases of the action potential (AP) repolarization process in HF to those in age-matched control. Magnitude of  $I_{Nife}$  at the early repolarization phase (phase 1) of the AP (at +40 mV) predominantly represents  $I_{CaL}$ , whereas the magnitude of  $I_{Nife}$  during the terminal repolarization (at -60 mV) is generated predominantly by the inward  $I_{NCX}$  (under physiological conditions). **A**  $I_{NaL}$  and  $I_{Nife}$  traces measured in control and HF under AP-clamp at 2 Hz pacing without using any  $Ca^{2+}$  buffer or  $\beta$ -adrenergic receptor ( $\beta AR$ ) agonist. Mean traces and SEM are shown. **B** When  $[Ca^{2+}]_i$  cycling is preserved, upregulation of  $I_{NaL}$  increased the net inward current during phase 3 of AP. **C**  $\beta AR$  stimulation using isoproterenol (ISO, 10 nmol/L) significantly upregulated not only  $I_{CaL}$  but also  $I_{NaL}$  and  $I_{NCX}$ . However, HF cells were hyporesponsive to ISO-induced stimulation (ie, both  $I_{CaL}$  and  $I_{NaL}$  increased in a smaller extent than in control), thus net inward current at +40 mV (predominantly  $I_{CaL}$ ) was significantly decreased in HF compared with control. Despite hyporesponsiveness, the net inward current during AP terminal repolarization was still significantly increased in HF because of the upregulated  $I_{NaL}$  and  $I_{NCX}$ . **D** CaMKII inhibition using the specific inhibitory peptide AIP largely diminished the difference between control and HF by reducing the upregulated  $I_{NaL}$  in HF. **E** Buffering  $[Ca^{2+}]_i$  (BAPTA<sub>i</sub>) eliminated the inward  $I_{NCX}$  and significantly decreased the extent of  $I_{NaL}$  enhancement in HF limiting the increase in net inward current. **F** Under  $\beta AR$  stimulation in BAPTA<sub>i</sub>, HF cells exhibited slightly decreased  $I_{CaL}$ , but similar  $I_{NaL}$  density compared to control. The contributions of these inward currents to total net charge are shown in insets.

Columns and bars represent mean $\pm$ SEM. Statistics and *n* numbers are shown in Figures 2 through 6.

Author Manuscript

Author Manuscript

Author Manuscript

Author Manuscript